RAI: Volume 3, Chapter 2.2.1.3.2, Number 1:

For the drip shield capacity assessment, provide a technical basis for not increasing the lateral loading as the vertical loading increases. This modeling assumption appears inconsistent with the implemented assumption that drip shield lateral resistance increases as vertical loading increases.

Basis: The model boundary conditions applied to the drip shield sides appear to unduly increase the structural resistance of the drip shield legs. To determine the system capacity, the model assumes the vertical loading of the original loading configuration can increase, but the active lateral rubble loading remains constant (SNL, 2007; Section 6.4.3.2.2.2). This assumption appears inconsistent with other information that indicates an expected increase in lateral load as the height of a rubble pile increases (e.g., BSC, 2004b, Table 5-29). Because of this modeling assumption, there is an increase in the tendency for outward deformation (i.e., "bowing) of the drip shield legs as only the vertical load increases. The applicant counteracts the bowing by applying a reactive lateral resistance whose stiffness is a function of the elastic modulus of the rubble (SAR Section 2.3.4.5.3.3.2).

1. RESPONSE

The lateral load in the drip shield capacity assessment does not have constant lateral loading. The capacity assessment for the drip shield framework incorporates a passive (reactive) pressure to represent the varying rubble load on the sidewalls of the drip shield due to large, inelastic lateral deformation. This approach provides a more accurate representation of the lateral rockfall load induced by large structural deformation than the lateral rockfall loads from the UDEC calculations (BSC 2004, Table 3), which assume an elastic drip shield with small deflections. The displacement-related change in lateral load eliminates the need to increase the lateral load as a function of the vertical load (i.e., as the height of the rubble pile increases). The response to this RAI also demonstrates that the vertical load is the primary load on the drip shield and explains why the quasi-static approach is expected to bound the dynamic response of the system.

1.1 LATERAL ROCKFALL LOADS ON THE DRIP SHIELD

Rocks that fall on the drip shield will consist of blocks of irregular shapes and various sizes. The manner in which the rock blocks fall and accumulate around the drip shield is a random process, and the distribution of the point loads on the drip shield will therefore vary in location and in magnitude due to the stochastic nature of drift degradation. The loading on the drip shield framework is a function of the magnitude of the load and its distribution on the drip shield surface. This distribution was discretized over 30 intervals of approximately equal length to account for the variability of loads on a cross-section of the drip shield surface (SNL 2007a, Section 6.4.3.2.2.2 and Figure 6-51).

The coupled response of the rubble/drip shield is a key element in accurate simulations of plastic load capacity. The analysis of plastic load capacity for the drip shield framework incorporated a passive (reactive) pressure to represent the changing rubble load on the sides of the drip shield due to large, inelastic lateral deformation. That is, as the sidewalls displace toward the rubble, the passive (reactive) lateral pressure of the rubble on the sidewalls increases (SNL 2007a, Section 6.4.3.2.2.3).

This approach provides a more accurate representation of the rockfall load induced by large, inelastic structural deformation than using a constant value for the lateral load. The constant values for lateral loading (as shown in BSC 2004, Table 3) are based on UDEC calculations with an elastic drip shield. This approach is reasonable for defining a factor of safety because drip shield deformations generally remain small until the onset of yielding. However, the plastic load capacity calculations involve large, inelastic deformation of the drip shield, and the UDEC calculations are not representative of these rockfall loads. The technical approach for calculating plastic load capacity uses a passive, reactive pressure to represent the changing rubble loads because large, inelastic deflections of the drip shield may produce large changes in lateral loading.

The ultimate plastic load capacity of the drip shield framework (i.e., the limit load at which the framework fails) was determined based on two load distributions: (a) an average of the six quasi-static rockfall loads, and (b) the loads for realization 3, which was selected because it has the maximum vertical load among the six generated cases (SNL 2007a, Section 6.4.3.2.2.2). The actual pressure distribution for the 30 discrete intervals was used to determine plastic load capacity for each case. Table 1 summarizes the static rubble loads on the left leg, top, and right leg of the drip shield for the six static rockfall cases and the average values for the six cases.

Table 1. Average Pressure Values on the Drip Shield for Quasi-static Drift Degradation

Realization	Pressure (kPa)		
	Left Leg	Top (Crown)	Right Leg
1	41.54	108.91	58.76
2	19.15	147.07	19.33
3	31.35	154.81	6.69
4	57.23	129.75	128.81
5	69.69	112.73	105.43
6	32.97	113.87	52.19
Average	41.99	127.86	61.87

Source: Adapted from SNL 2007a, Table 6-136.

In the computational methodology (SNL 2007a, Sections 6.4.3.2.2.2 and 6.4.3.2.2.3), the two initial load realizations (load realization 3 and the average of six load realizations) were modified to account for the increased vertical load of the rubble during a seismic event. The vertical load on the drip shield (on intervals 11 through 20 in Figure 6-51 of SNL 2007a) was gradually increased proportionally to the initial load distribution. The initial lateral loads on the drip shield legs were not increased with the vertical load, but were a function of sidewall displacement. The reactive rubble pressure resulting from lateral deformation of the drip shield sidewalls

was superimposed on the initial pressure distribution only at locations where the sidewalls moved toward the rubble; elsewhere the lateral pressure does not change (SNL 2007a, Section 6.4.3.2.2.3). If greater vertical loading results in more outward bowing of the sidewalls, then the lateral pressure of the rubble on the sidewalls is also increased as a function of lateral displacement. This approach is more realistic than representing the lateral load on the drip shield as a constant dead weight of the rubble, which does not increase with outward bowing of the sidewalls. This approach is also more realistic because the reactive load is not applied for inward bowing of the sidewalls, when lateral rockfall load may decrease and the lower initial values for lateral load may be more appropriate. The displacement-related change in lateral load eliminates the need for an increase in static lateral load using a density multiplier.

Previous quasi-static calculations assessed the factor of safety of the drip shield under quasi-static pressure (BSC 2004, Section 6). For these quasi-static analyses, an increase in the density of rubble in the two-dimensional analysis of drip shield–rubble interaction was used as a method to generate increased rubble loads on the drip shield. This new load distribution was then applied to a three-dimensional, elastic-plastic representation of a slice of the drip shield to assess its stability under increased vertical loads. Table 2 presents the average pressures as a function of the density multiplier.

Table 2. Average Pressure Values on the Drip Shield as a Function of Rubble Density

Density Multiplier	Pressure (kPa)		
	Left Leg	Top (Crown)	Right Leg
1	41.99	127.86	61.87
2.5	69.86	263.73	80.98
3	82.98	314.81	89.54
4	105.74	415.97	109.03

Sources: SNL 2007a, Table 6-136, for the average of six realizations for the density multiplier of 1; BSC 2004, Table 3, for density multipliers greater than 1.

Figure 1 is a plot of the data in Table 2. Figure 1 demonstrates that the variability of the vertical rockfall load is much greater than the variability of the lateral rockfall load as a function of the density multiplier.

The assessment of the plastic load capacity of the drip shield framework (SNL 2007a, Sections 6.4.3.2.2.2 and 6.4.3.2.2.3) focuses on vertical loading because the vertical rockfall load is significantly greater than the lateral load, based on the results in Figure 1. In addition, the classical analysis for buckling of a thin beam determines the stability of the beam under thrust, i.e., for a force parallel to the beam and applied at its end(s). The corresponding load for buckling the sidewalls is the vertical load on the crown.

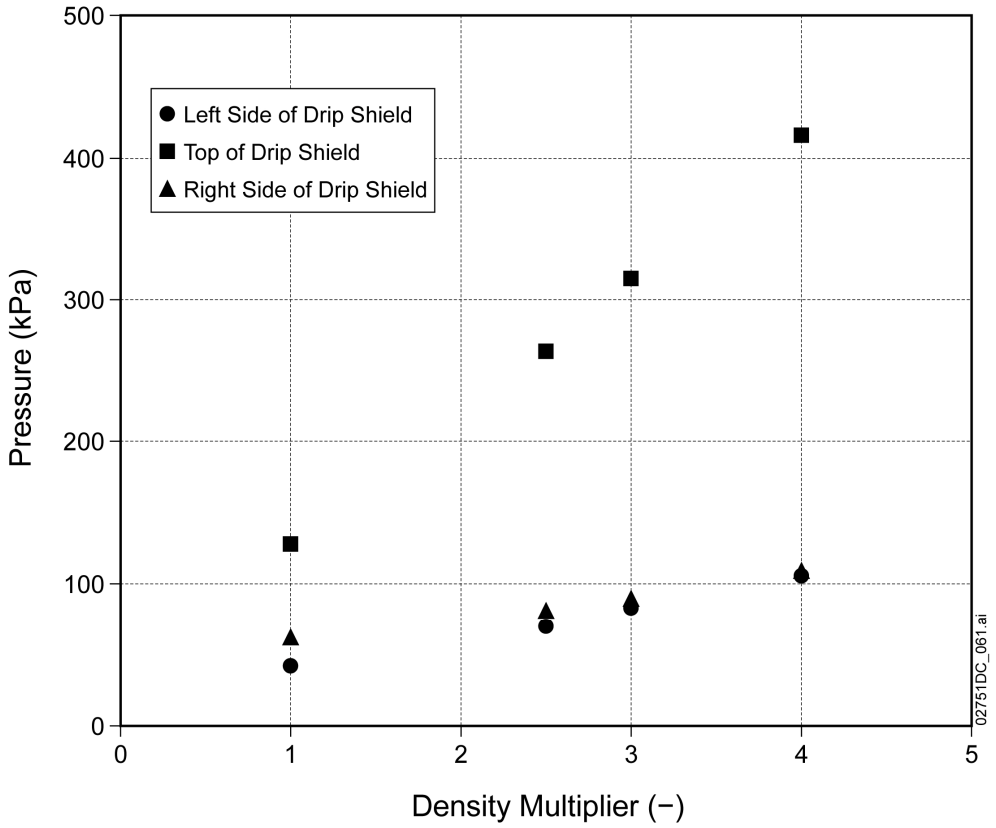

Figure 1. Average Rockfall Pressure on the Sides and Top of the Drip Shield as a Function of the Density Multiplier

1.2 CONSERVATISM IN FRAGILITY CURVES

The fragility curves for the drip shield framework require a relationship between the vertical quasi-static load that causes the sidewalls to buckle and the dynamic rockfall/drip shield load during vibratory ground motion. Vibratory ground motion will result in an amplification of the static rubble load on the drip shield. This amplification is taken into account by relating the vertical quasi-static load that causes buckling to the maximum vertical load amplification during the ground motion (SNL 2007b, Equation 6.8-1). Mathematically,

$$(Quasi\text{-}Static\ Load)_v \equiv (Rubble\ Load)_v(1 + (PGA_v)/g) \quad \text{(Eq. 1)}$$

where PGA is the peak ground acceleration (measured in g's) and the subscript v denotes the vertical component. This definition is only true at the single point in time when the vertical ground acceleration reaches its maximum value of PGA_v. That is,

$$(Quasi\text{-}Static\ Load)_v \geq (Rubble\ Load)_v(1 + A_v(t)/g) \quad \text{(Eq. 2)}$$

where $A_v(t)$ is the time-dependent vertical ground acceleration. In other words, the quasi-static load is greater than the amplified static rubble load, except when the vertical ground acceleration equals its peak value of PGA_v. In addition, the quasi-static load is always greater than the

right-hand side of Equation 2 if PGA_v occurs during a downward (negative) acceleration which decreases (rather than increases) the vertical load on the drip shield. The quasi-static load in Equation 2 is therefore expected to provide an upper bound to the dynamic load on the drip shield from vibratory ground motion. This expectation has been confirmed by the results from fully dynamic calculations for rockfall/drip shield response to vibratory ground motion (SAR Section 2.3.4.5.3.3.3). The dynamic calculations make no explicit assumptions about the dynamic behavior of the vertical and lateral loads relative to the static rockfall load.

1.3 CONSISTENCY WITH RELATED FEPS

The analysis of plastic load capacity for the drip shield framework incorporated a passive (reactive) pressure to represent the varying rubble load on the sides of the drip shield due to its lateral deformation during a seismic event. This is a physically reasonable approach for the drip shield capacity assessment. This approach is not relevant to the screening justifications for excluded FEPs 2.1.07.05.0B, Creep of Metallic Materials in the Drip Shield; 2.1.03.03.0B, Localized Corrosion of Drip Shields; 2.1.06.05.0B, Mechanical Degradation of Invert; and 2.1.07.06.0A, Floor Buckling.

1.4 CONCLUSIONS

- The assessment of the plastic load capacity of the drip shield framework (SNL 2007a, Sections 6.4.3.2.2.2 and 6.4.3.2.2.3) focuses on vertical loading because the vertical load on the crown is the driving force for lateral buckling of the sidewalls and because the average vertical rockfall load is significantly greater than the average lateral rockfall load, based on the results in Figure 1.

- The quasi-static vertical load on the drip shield, as defined in Equation 2, provides an upper bound to the dynamic vertical load on the drip shield from static rockfall and vibratory ground motion. This expectation has been confirmed by the results from fully dynamic calculations for rockfall/drip shield response to vibratory ground motion (SAR Section 2.3.4.5.3.3.3). The dynamic calculations make no explicit assumptions about the dynamic behavior of the time-dependent vertical and lateral loads during a seismic event.

- The analysis of plastic load capacity for the drip shield framework incorporated a passive (reactive) pressure to represent the varying rubble load on the sides of the drip shield due to large, inelastic lateral deformation during a seismic event. This approach provides a more accurate representation of the lateral rockfall load induced by large structural displacement than the UDEC model, which assumes an elastic drip shield with small deflections. The displacement-related change in lateral load eliminates the need to increase the lateral load as a function of the density multiplier (i.e., as the height of the rubble pile increases).

2. COMMITMENTS TO NRC

None.

3. DESCRIPTION OF PROPOSED LA CHANGE

None.

4. REFERENCES

BSC 2004. *Structural Stability of Drip Shield Under Quasi-Static Pressure*. 000-00C-SSE0-00500-000-00A. Las Vegas, Nevada: Bechtel SAIC Company. ACC: ENG.20040830.0032.

SNL 2007a. *Mechanical Assessment of Degraded Waste Packages and Drip Shields Subject to Vibratory Ground Motion*. MDL-WIS-AC-000001 REV 00. Las Vegas, Nevada: Sandia National Laboratories. ACC: DOC.20070917.0006.

SNL 2007b. *Seismic Consequence Abstraction.* MDL-WIS-PA-000003 REV 03. Las Vegas, Nevada: Sandia National Laboratories. ACC: DOC.20070928.0011.

RAI Volume 3, Chapter 2.2.1.3.2, Number 2:

Demonstrate that the inclusion of model lateral constraints, representing the pallet base over the entire length of the drip shield, does not inappropriately bias the drip shield response in the analysis. Alternatively, provide a separate structural analysis for the drip shield segments that do not contact the pallet base.

Basis: The representative drip shield section of the applicant's model includes a lateral constraint to represent the base of the emplacement pallet (SAR Figure 2.3.4-74). The length of the base pallet, however, is approximately one fifth of the drip shield length.

1. RESPONSE

1.1 INTRODUCTION

The lateral constraint representing the pallet does not inappropriately bias the drip shield response in the analyses. It will be shown in this response that in most of the calculations the contact between the drip shield and the lateral constraint does not take place. It is also demonstrated that in the cases when the contact occurs, the waste package supports and the stainless steel tubes of the emplacement pallet can support the interaction force.

The lateral constraint that represents the emplacement pallet is included in the numerical analyses of the drip shield statically loaded by rock rubble (BSC 2004), creep deformation of the drip shield under static rubble load (BSC 2005), and drip shield fragility (SNL 2007, Section 6.4.3.2). The geometry of the drip shield representation used in those calculations is shown in Figure 1. The numerical representations include only one typical segment of the drip shield—i.e., the typical framework with plates extending to the symmetry planes between the adjacent frameworks. The drip shield, which is 5.805-m long, includes four typical segments. The end framework, where the pallet does not extend, is non-typical because it is overlapped between two adjacent, interlocking drip shields, and is reinforced by support beam connectors on both drip shields at the overlap, instead of support beams found in the typical segments on the drip shield sides.

The lateral constraints, assumed to be rigid in the numerical representations, represent the emplacement pallet—specifically, the upper portion of the waste package support (pallet base) and the stainless steel tubes between the two waste package supports. The total length of the standard (long) pallet is 4.148 m. The length of two waste package supports at the pallet ends is 0.5429 m. Thus, the length of the stainless steel tubes between the waste package supports is 3.06 m. The discussion in this response is for the standard pallet, which accounts for approximately 90% of the pallets in the repository. The remaining 10% are the short pallets, 2.501-m long. The proportion of the repository length with the short pallets is less than 10%, because they are shorter than the standard pallets.

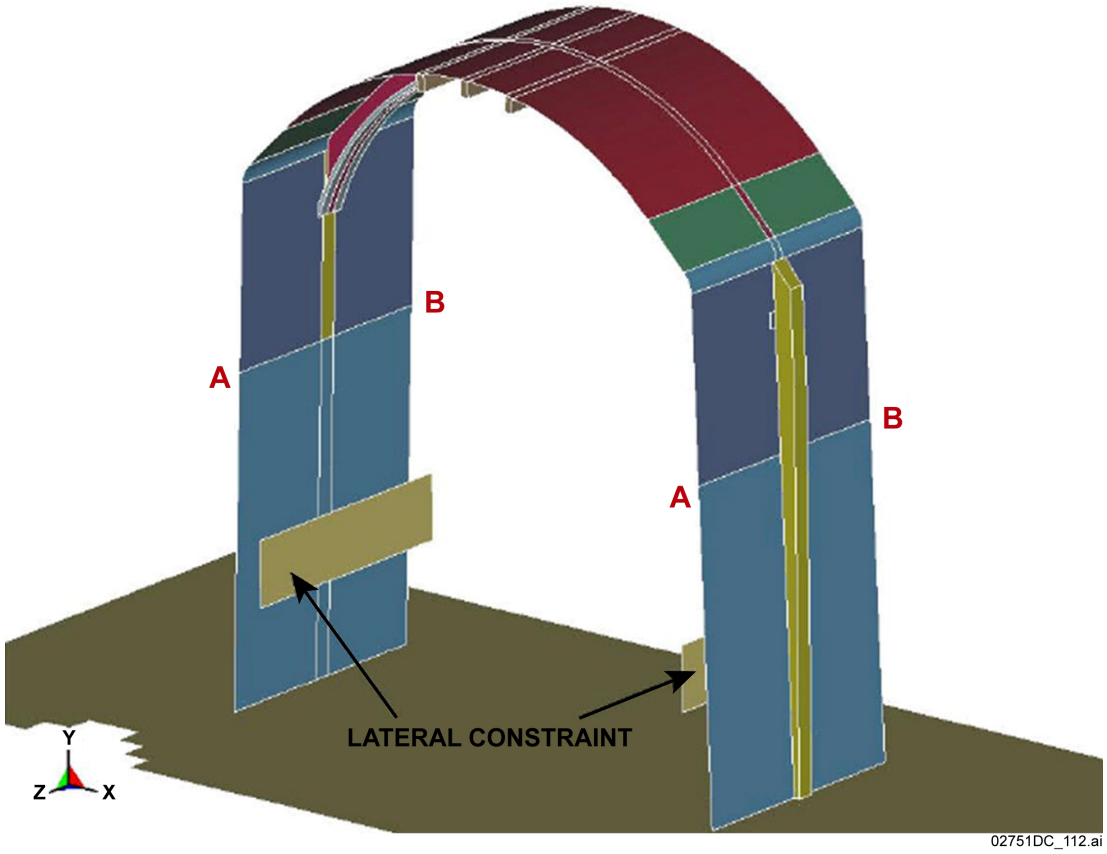

Source: BSC 2004, Figure 2.

Figure 1. Geometry of the Drip Shield Representations in LS-DYNA and FLAC3D Calculations

An inappropriate bias of predicted drip shield response due to lateral constraints in the model will occur if: (1) the model predicts contact between the drip shield and the lateral constraint, and (2) the object represented by the lateral constraint either does not exist or it cannot sustain the interaction force between the drip shield and the lateral constraint. The lateral constraints represent the emplacement pallets, both the waste package supports and the stainless steel tubes between the supports. The emplacement pallet extends along 71% of the total drip shield length, or approximately along the entire length of four typical segments (which is 4.3 m as the single segment length is 1.072 m) considered in the analyses. (Relevant dimensions and spatial relations between the drip shield and the pallet are illustrated in Figure 1a.) The remaining 29% of the drip shield length that does not have the emplacement pallet to potentially lean on, if they do not correspond to stronger, overlapped end-segments, will deform more than the sections with the lateral constraints, resulting in both load redistribution of surrounding rubble on the drip shield but also some redistribution of stresses within the drip shield, as it will respond as a three-dimensional structure. Clearly, the structure and size of the waste package supports on which the waste package is resting are such that the potential interaction forces between the drip shield and the emplacement pallet will support the drip shield without significant deformation. In addition, as demonstrated in Section 1.2, the stainless steel tubes extending between the waste package supports also will be able to sustain the interaction forces. Thus, the lateral constraints

included in the analyses adequately represent the interaction between the drip shield and the pallet. Detailed discussion of the interaction between the drip shield and the pallet, and response of the pallet, is presented in Section 1.2.

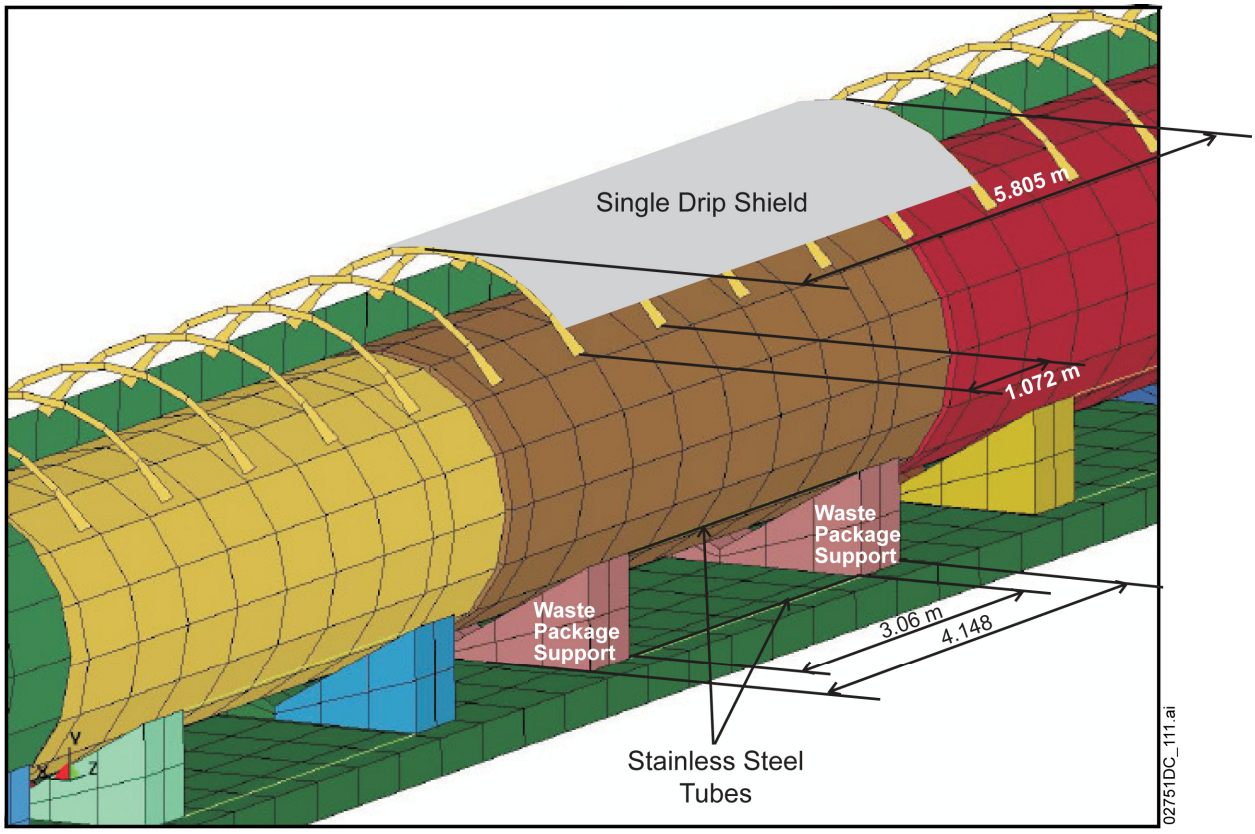

Source: For illustrative purposes only.

Figure 1a. Illustration of the Drip Shield and the Emplacement Pallet with Relevant Dimensions

1.2 DISCUSSION

1.2.1 Static Rubble Load

The analysis of drip shield deformation and stability shows that there is no contact between the drip shield and the lateral constraints when the drip shield is loaded with rubble resulting from a fully collapsed drift in the lithophysal units. Visual inspection of the drip shield configurations in *Structural Stability of a Drip Shield Under Quasi-Static Pressure* (BSC 2004, Attachment II, Figures II-1 through II-6) confirms that the drip shield does not touch the lateral constraint. Even in the case of the factor-of-safety calculations, carried out for 2.5, 3.0, and 4.0 times increased rubble density, the drip shield and the lateral constraint do not touch (BSC 2004, Attachment II, Figures II-7 through II-9).

Thus, the representation of the emplacement pallet as a lateral constraint does not affect the results regarding the drip shield stability and factor of safety under static load of accumulated rubble in the collapsed drifts in the lithophysal rock mass. (The static rubble loads in the lithophysal units overestimate the static rubble loads in the nonlithophysal units.)

1.2.2 Drip Shield Fragility

The analysis of the drip shield fragility (SNL 2007, Section 6.4.3.2) was conducted by gradually increasing the vertical load in relatively small, equal increments until the drip shield collapsed (i.e., SNL 2007, Figures 6-54 through 6-56). The analysis was carried out for the average of the six load realizations (the vertical average pressure of 127.86 kPa) and load realization 3 (the maximum vertical average pressure of 154.81 kPa). The exact load at which the drip shield collapsed was determined from the intersection of the maximum effective plastic strain as a function of the drip shield load with the threshold corresponding to the failure strain (SNL 2007, Figure 6-53).

The model states are saved in files at the finite load increments. Inspection of the model configurations indicates that in five of the six analyzed cases, the drip shield touches the pallet only when the drip shield is already in the state of failure and has undergone large deformation as a result of strains that exceed the failure strain. Figures 2 through 7 show the six model configurations (for two different loads and 3 drip shield configurations, chosen to represent different stages of thinning of drip shield components due to uniform corrosion) in states very close to but less than the failure loads. Table 1 lists the failure loads for the six analyzed cases and the loads in the states shown in Figures 2 through 7. Only in the case of the drip shield configuration with 5-mm thick plates loaded by the average rubble load does the drip shield touch the emplacement pallet before the drip shield reaches the failure state (either by buckling of the legs or by buckling of the crown). However, considering the trend of the fragility curve for the average load in *Mechanical Assessment of Degraded Waste Packages and Drip Shields Subject to Vibratory Ground Motion* (SNL 2007, Figure 6-57) and Table 1, the contact between the drip shield and the pallet has an insignificant effect on the limit load calculated for that case. The case for the configuration with 5-mm thick plates is on the same trend line (in the failure load versus plate thickness plot; SNL 2007, Figure 6-57) as defined by failure loads from configurations with 10-mm and 15-mm thick plates. This is confirmed further by the observation that the limit load for the same configuration but for load realization 3, in which the contact between the drip shield and the pallet does not occur until the drip shield fails, is greater than that for the average load (Table 1).

Therefore, the lateral constraints included in the model used for drip shield fragility calculations do not affect the drip shield response in the analysis.

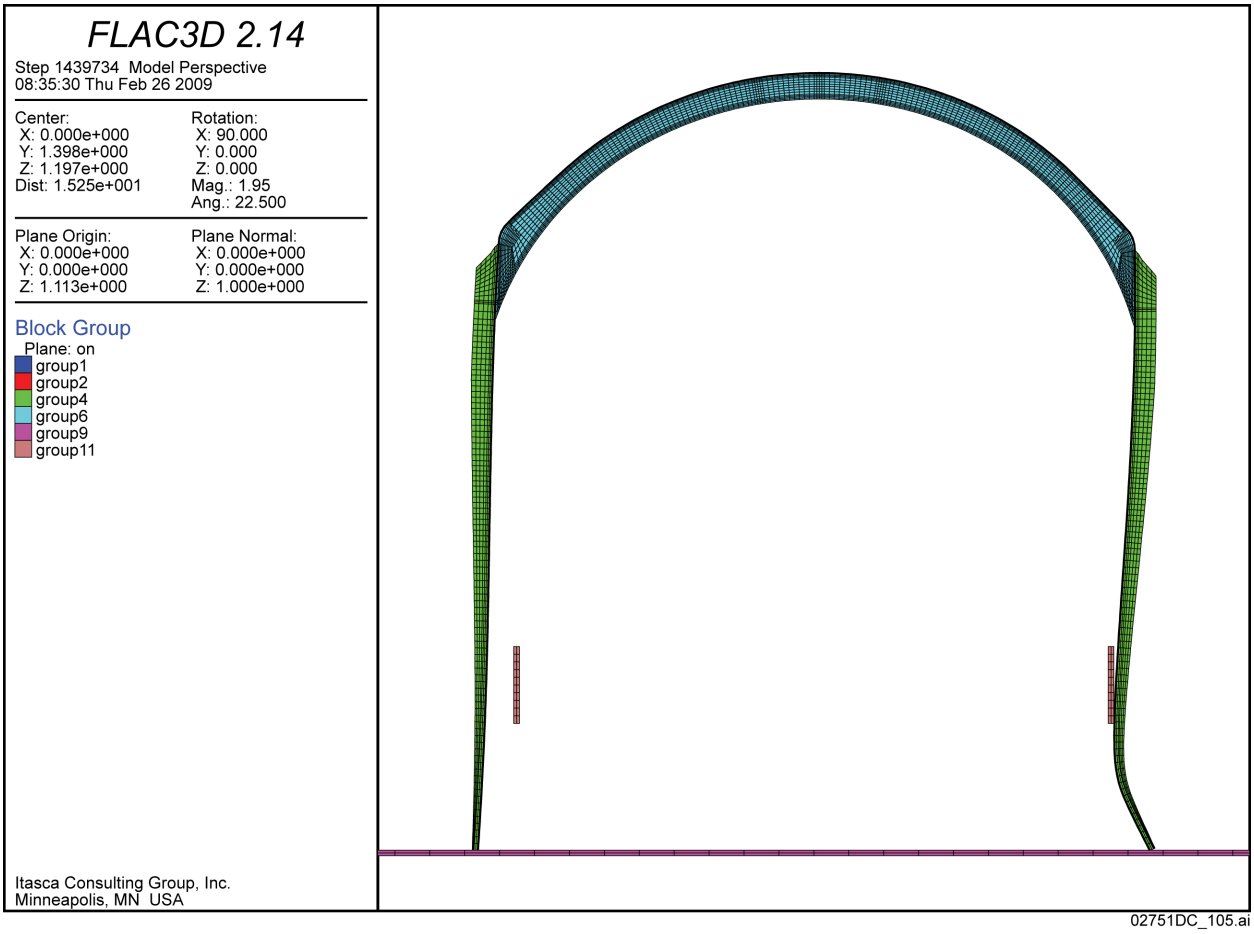

Figure 2. Drip Shield Configuration for 5-mm Thick Plates and Average Load Amplified 3.8 Times in the Vertical Direction (figure dimensions in meters)

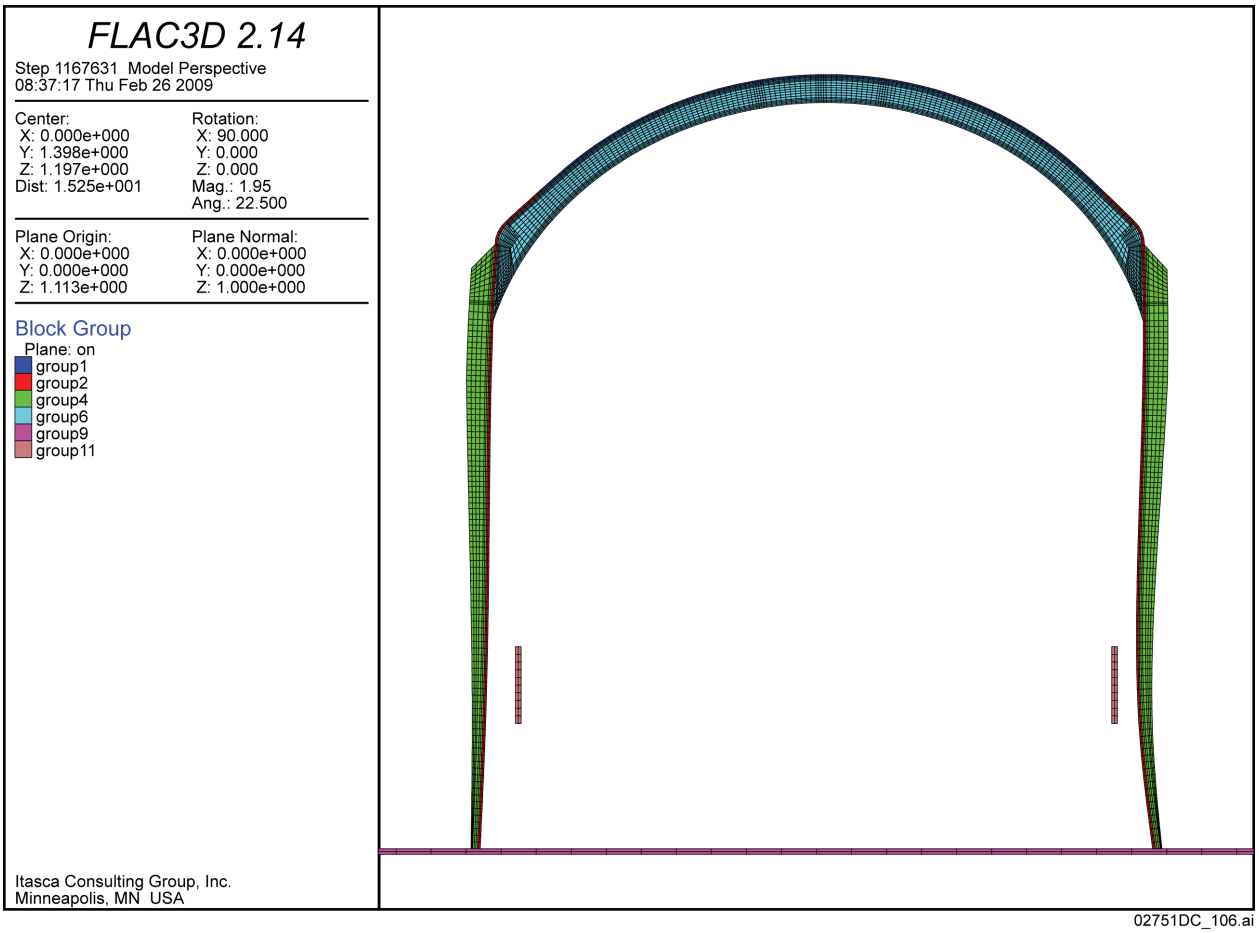

Figure 3. Drip Shield Configuration for 10-mm Thick Plates and Average Load Amplified 8.3 Times in the Vertical Direction (figure dimensions in meters)

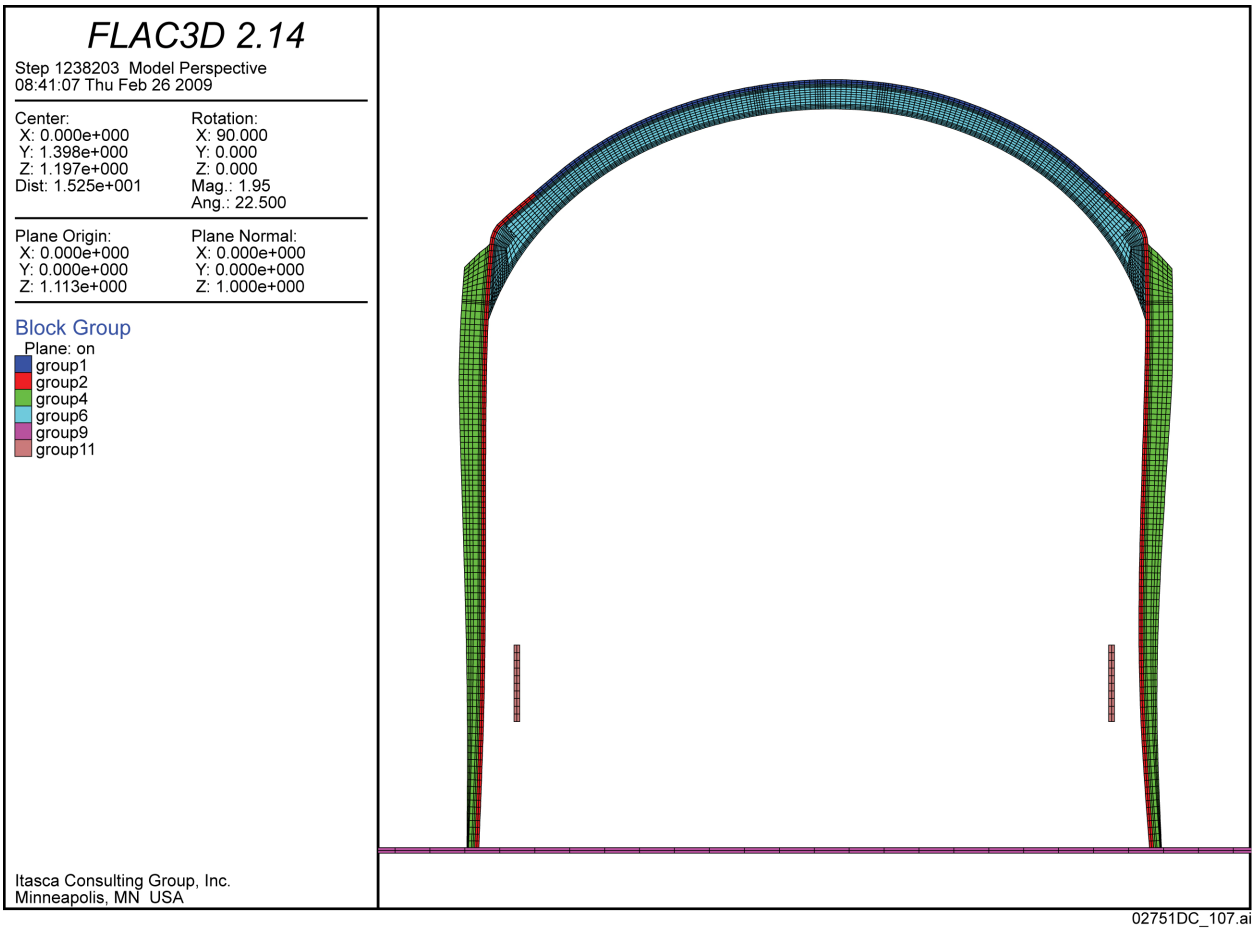

Figure 4. Drip Shield Configuration for 15-mm Thick Plates and Average Load Amplified 13.2 Times in the Vertical Direction (figure dimensions in meters)

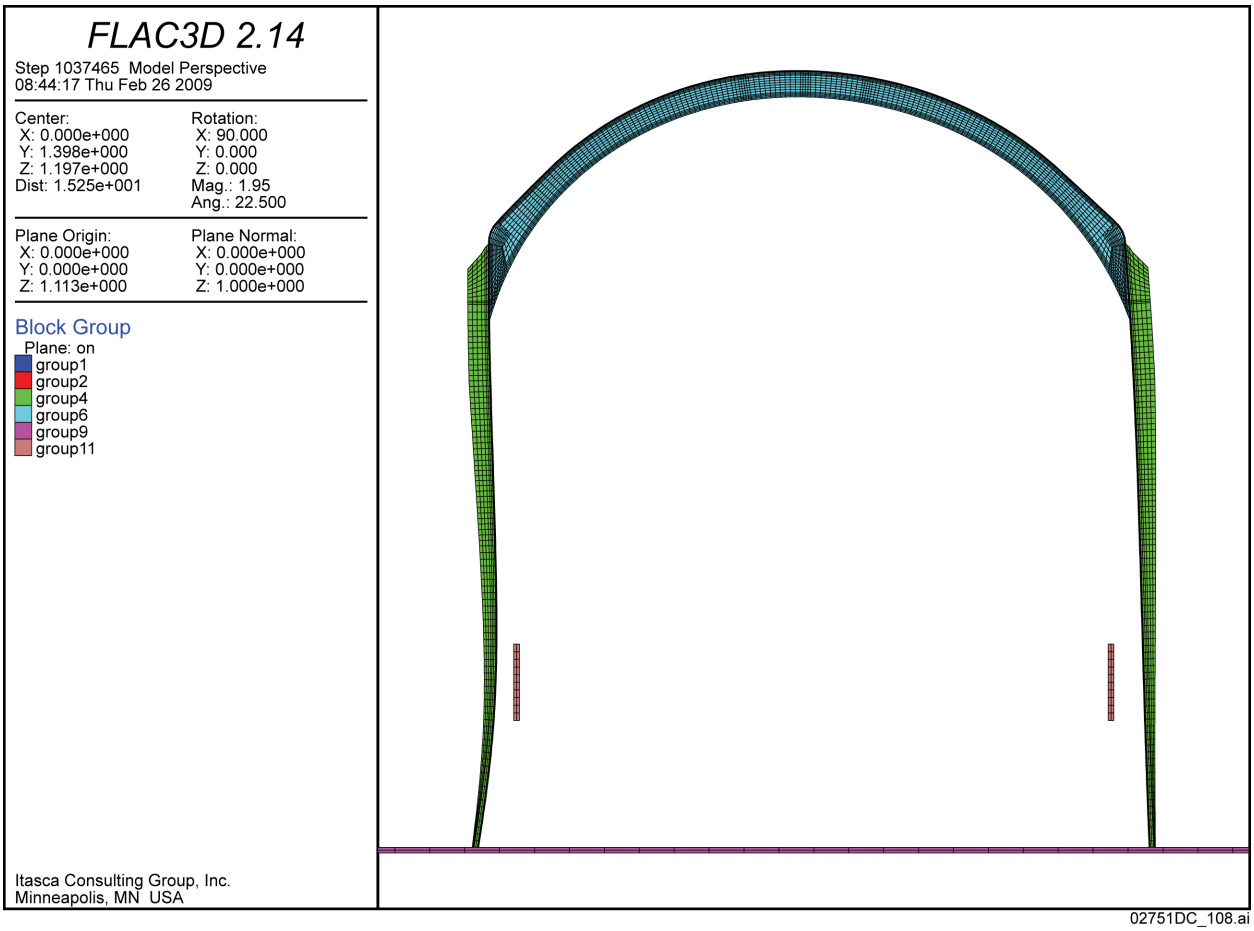

Figure 5. Drip Shield Configuration for 5-mm Thick Plates and Load Realization 3 Amplified 3.8 Times in the Vertical Direction (figure dimensions in meters)

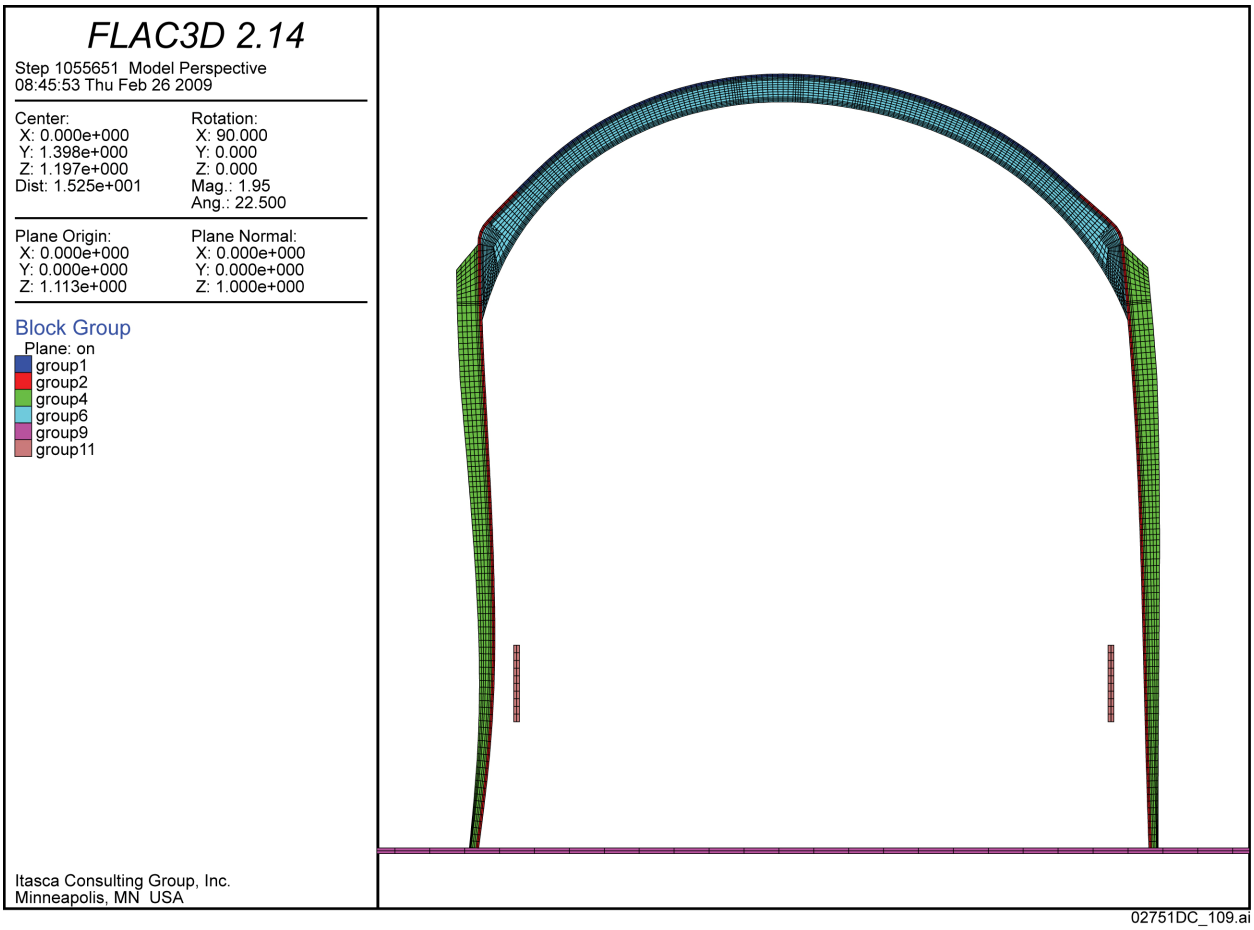

Figure 6. Drip Shield Configuration for 10-mm Thick Plates and Load Realization 3 Amplified 7.4 Times in the Vertical Direction (figure dimensions in meters)

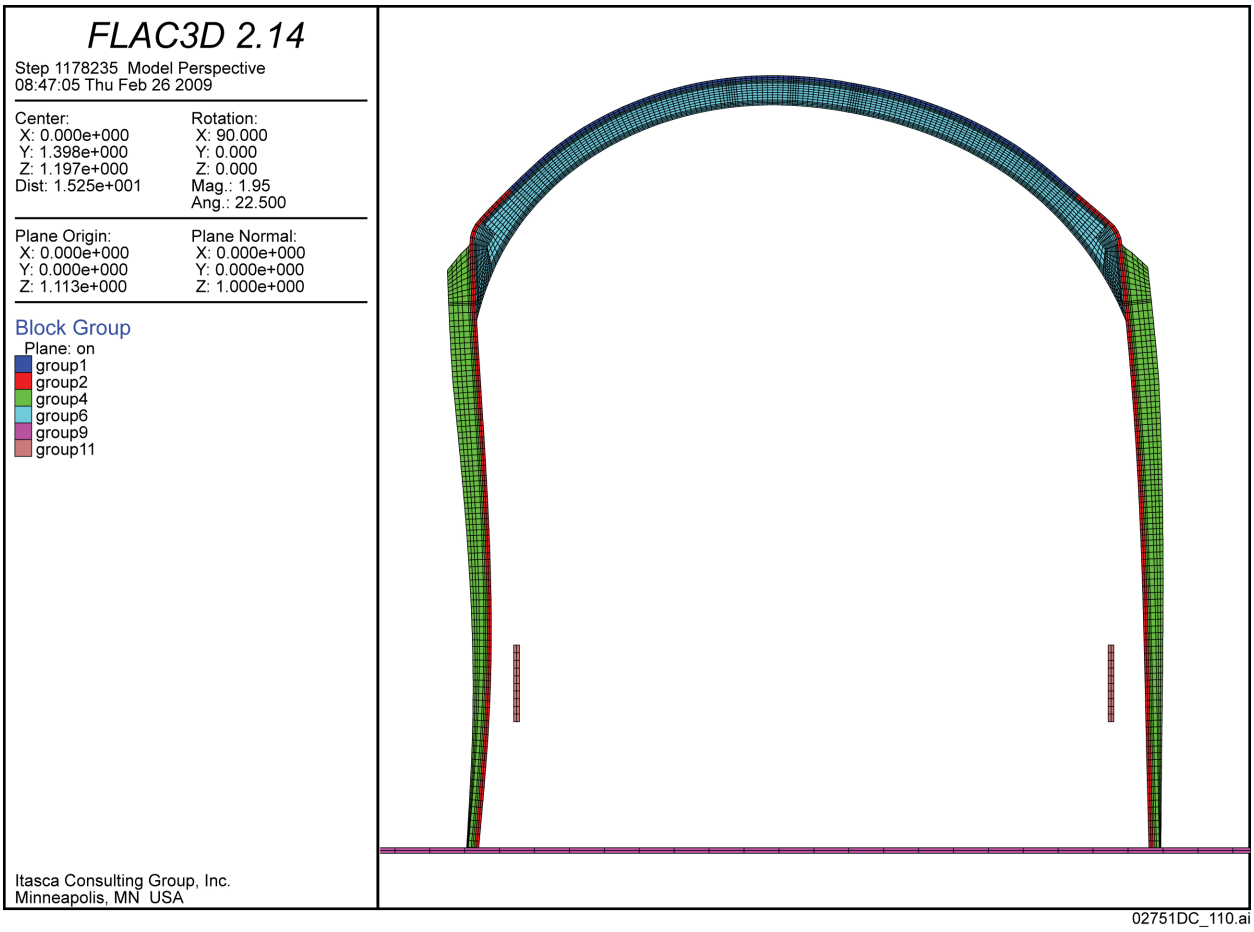

Figure 7. Drip Shield Configuration for 15 mm Thick Plates and Load Realization 3 Amplified 10.3 Times in the Vertical Direction (figure dimensions are in meters)

Table 1. Comparison of the Failure Loads with the Loads for the States Shown in Figures 2 through 7

Plate Thickness (mm)	Loads in States Shown in Figures 2 through 7 (kPa)*		Failure Loads (kPa)	
	Load Realization 3	Average Load	Load Realization 3	Average Load
5	588	486	606	501
10	1,146	1,061	1,183	1,094
15	1,595	1,688	1,622	1,698

Source: Loads in * calculated by multiplying the vertical loads for realization 3 of 154.81 kPa (SNL 2007, Table 6-136), and the average load of 127.86 kPa (SNL 2007, Table 6-136) by factors indicated in Figures 2 through 7.

1.2.3 Creep Deformation of the Drip Shield

The analysis of the drip shield deformation due to creep of titanium for 10,000 years indicates that the drip shield leg touches the lateral constraint at the end of the simulation (BSC 2005, Figures 5.4-8 through 5.4-13). The values of the forces between the drip shield and the lateral constraint at the end of creep simulations have been extracted from the analysis output files, and the distributed linear loads on the pallet are calculated by averaging the forces over the length of the drip shield segment (1.072 m). The distributed loads, listed in Table 2, indicate significant variability, between no load for load realization 3 and 166.8 kN/m for load realization 4. A comparison indicates a strong correlation between the distributed linear loads in Table 2, with average rubble pressures on the drip shield legs (BSC 2005, Table 5.2-2). For example, the maximum lateral loads on the drip shield legs and the distributed loads on the pallet are for load realizations 4 and 5. The minimum lateral load is for load realization 3. The load distributions, as provided by the six load realizations, will not extend along the entire length of the segment and certainly not along the entire length of the drip shield. (Different rubble load realizations represent possible variability of rubble load that can occur at a distance less than a meter.) Because of the size of the rock blocks in the rubble (i.e., of the order of a fraction of a meter), the load will vary along the drip shield, resulting in less variability when averaged over the length of the drip shield segment. The analyses were conducted conservatively assuming that the six load realizations act along the entire length of the drip shield segment. Consequently, the extreme values of distributed loads obtained from the six rubble load realizations overestimate or underestimate the drip shield load in the connecting beam. The average value, also listed in Table 2, is a better representation of typical distributed load on the pallet than any of the values for the six load realizations.

In order to estimate whether the 3.06-m long stainless steel tubes can sustain the loads of the leaning drip shield, the maximum moments due to distributed loads are calculated representing the stainless steel tubes as a beam fixed at both ends. The maximum moments, calculated assuming elastic beam response (i.e., because the stainless steel tubes are clamped at the ends $M = ql^2/12$, where q is the distributed load and l is the span) and formation of three plastic hinges ($M = ql^2/16$ as the moment is equally divided between the hinges at the support and in the middle of the beam), are listed in Table 2.

Table 2. Load on the Stainless Steel Tube and Maximum Moments Assuming Elastic and Plastic Deformation of the Beam

Load Realization	Distributed Load on Beam (kN/m)	Maximum Elastic Moment (kNm)	Maximum Plastic Moment (kNm)
1	4.0	3.1	2.3
2	34.7	27.1	20.3
3	0.0	0.0	0.0
4	166.8	130.2	97.6
5	152.3	118.8	89.1
6	28.1	21.9	16.5
Average	64.3	50.2	37.6

The moment capacities, corresponding to the onset of yielding in the stainless steel tube and ultimate load when the beam fails, are listed in Table 3. The stainless steel tubes are square tubes, 6 in × 6 in (outside dimensions), with 0.375-in (9.5-mm) wall thickness (stainless steel, SA-240-S31600). The wall thickness is estimated to decrease approximately 1.8 mm (0.07 in) due to corrosion over 10,000 years (SNL 2008, FEP 2.1.06.05.0C). The yield strength of 193 MPa and ultimate tensile strength of 517 MPa for stainless steel at 60°C (SNL 2007, Section A3) were used to calculate the maximum moment capacities. A temperature of 60°C was used to represent conditions 10,000 years after closure (SNL 2007, Section 5.7), when the forces are recorded.

Comparison of the estimated bending moments (Table 2) and the moment bearing capacities (Table 3) indicates that the average load will cause yielding of the stainless steel tube, but will not fail the beam (measured against the plastic moment). The loads on the stainless steel tube for four rubble load realizations (1, 2, 3, and 6) will not cause yielding of the stainless steel tube in either initial or thinned configurations. Even the greatest load on the stainless steel tube (load realization 4) will not fail the stainless steel tube thinned by corrosion over 10,000 years (i.e., 97.6 MPa < 107.7 MPa). The creep analysis with rigid lateral constraints representing yielding stainless steel tubes will insignificantly underestimate the creep strains. Considering that the maximum strains calculated from the creep calculation (BSC 2005, Section 5.4.3 and Table 5.4-1) are much smaller than the failure threshold strains, deformation of the stainless steel tubes is inconsequential for the conclusions of creep analyses.

Table 3. Maximum Moment Capacities of the Stainless Steel Tube

	Maximum Elastic Moment (kNm)	Maximum Plastic Moment (kNm)
Initial Configuration	47.1	135.5
Configuration Thinned 1.8 mm	37.6	107.7

The stainless steel tube of the emplacement pallet will be capable of sustaining the loads estimated from the interaction between the drip shield and pallet. Thus, the representation of the emplacement pallet as a lateral constraint adequately approximates the interaction between the drip shield and pallet, and does not affect the results of the creep calculations inappropriately.

1.3 CONSISTENCY WITH RELATED FEPS

The inclusion of model lateral constraints, representing the pallet base over the entire length of the drip shield, does not inappropriately bias the drip shield response in the analysis. This approach is not relevant to the screening justifications for excluded FEPs 2.1.07.05.0B, Creep of Metallic Materials in the Drip Shield; 2.1.03.03.0B, Localized Corrosion of the Drip Shield; 2.1.06.05.0B, Mechanical Degradation of Invert; and 2.1.07.06.0A, Floor Buckling.

1.4 SUMMARY

The inclusion of the model lateral constraint, representing the pallet, does not bias the drip shield response analysis inappropriately. In the analyses of drip shield stability and factor of safety for static rubble load (BSC 2004) and drip shield fragility (SNL 2007), the contact between the drip shield and the representation of the pallet does not occur or is inconsequential. In the analysis of the creep deformation of the drip shield (BSC 2005), it is predicted that the drip shield will lean and contact the pallet. The analysis in Section 1.2.3 shows that the stainless steel tubes will sustain the interaction loads. With regard to creep analysis, the representation of the emplacement pallet as a lateral constraint adequately approximates interaction between the drip shield and pallet, and does not affect the results of the calculations inappropriately.

2. COMMITMENTS TO NRC

None.

3. DESCRIPTION OF PROPOSED LA CHANGE

None.

4. REFERENCES

BSC (Bechtel SAIC Company) 2004. *Structural Stability of a Drip Shield Under Quasi-Static Pressure*. 000-00C-SSE0-00500-000-00A. Las Vegas, Nevada: Bechtel SAIC Company. ACC: ENG.20040830.0032; ENG.20080312.0017.

BSC 2005. *Creep Deformation of the Drip Shield*. CAL-WIS-AC-000004 REV 0A. Las Vegas, Nevada: Bechtel SAIC Company. ACC: DOC.20050830.0007.

SNL (Sandia National Laboratories) 2007. *Mechanical Assessment of Degraded Waste Packages and Drip Shields Subject to Vibratory Ground Motion*. MDL-WIS-AC-000001 REV 00. Las Vegas, Nevada: Sandia National Laboratories. ACC: DOC.20070917.0006; DOC.20080623.0002; DOC.20081021.0001.

SNL 2008. *Features, Events, and Processes for the Total System Performance Assessment: Analyses*. ANL-WIS-MD-000027 REV 00. Las Vegas, Nevada: Sandia National Laboratories. ACC: DOC.20080307.0003; DOC.20080407.0009; LLR.20080522.0166; DOC.20080722.0002.

RAI Volume 3, Chapter 2.2.1.3.2, Number 3:

Provide a technical basis to demonstrate that the effect of loading configuration uncertainty on the drip shield capacity is appropriately represented by the two load cases used in SAR Section 2.3.4.5.3.3.2.

Basis: The applicant assessed drip shield performance under static loading using two loading configurations, which are derived from a set of six configurations for representing static rubble loading for complete drift collapse (SAR Section 2.3.4.5.3.3.2). The applicant used loading case 3, which the applicant stated is the most severe configuration, and the average of the six load cases. According to the applicant, the drip shield performance is relatively insensitive to different loading configurations and two loading cases are sufficient to characterize the system response. Nevertheless, analyses (BSC, 2004a) indicate that the lateral-to-vertical load ratio and asymmetry in the loading configurations may significantly modify the drip shield response.

1. RESPONSE

The effect of loading configuration uncertainty on drip shield framework capacity is appropriately represented by the two load cases used in SAR Section 2.3.4.5.3.3.2. Load realization 3 is not considered a maximal or severe load pattern, but is used to estimate +1 standard deviation in the plastic load capacity. This is appropriate because the magnitude of the vertical load on the crown for load realization 3 is 5% greater than +1 standard deviation above the average vertical load for the six load realizations, and because the resulting uncertainty is propagated forward into the framework fragility curves in a manner that maximizes the variability in plastic load capacity for the 5-mm and 0-mm thickness reductions, as demonstrated by Figure 2 of this response.

1.1 UNCERTAINTY IN THE STATIC ROCKFALL LOADING

The ultimate plastic load capacity of the drip shield framework (i.e., the limit load at which the framework fails) is based on two load distributions: (a) an average of the six quasi-static rockfall loads, and (b) the loads for realization 3, which was selected because it has the greatest load on the top (crown) of the drip shield among the six load realizations (SNL 2007a, Section 6.4.3.2.2.2). Table 1 presents the static rubble loads on the left leg, top (crown), and right leg of the drip shield, the average values for the six static rockfall realizations, and the standard deviations for the six realizations.

Table 1. Average Pressure Values on the Drip Shield for Quasi-static Drift Degradation

Realization	Pressure (kPa)		
	Left Leg	Top (Crown)	Right Leg
1	41.54	108.91	58.76
2	19.15	147.07	19.33
3	31.35	154.81	6.69
4	57.23	129.75	128.81
5	69.69	112.73	105.43
6	32.97	113.87	52.19
Average	41.99	127.86	61.87
Standard Deviation	18.53	19.40	47.62

Source: Adapted from SNL 2007a, Table 6-136.

The choice of the average of the six quasi-static rockfall loads to represent the average load on the drip shield framework is straightforward and is not discussed further.

The choice of realization 3 from the six load realizations is motivated by several considerations:

- The vertical load on the top (crown) is the driving force for lateral buckling of the sidewalls. The classical analysis for the buckling of a thin beam determines the stability of the beam under thrust (i.e., for a force parallel to the beam and applied at its end(s)). The corresponding load for buckling of the sidewalls is the vertical load on the crown.

- The average vertical rockfall load is significantly greater than the average lateral rockfall load, using dense rubble as an analogue for increasing dynamic loads, as explained below.

- The loading from realization 3 has the lowest lateral load on the right side and next to the lowest lateral load on the left side, as shown in Table 1. This loading configuration generally has the maximum differential between the vertical load on the crown of the drip shield and the lateral loads on the sidewalls, thereby providing the least restoring force for an asymmetric failure mode as the sidewalls bow out into the surrounding rubble.

Previous quasi-static calculations assessed the factor of safety of the drip shield under quasi-static pressure (BSC 2004). For these quasi-static analyses, an increase in the density of rubble in the two-dimensional UDEC analysis of rubble interaction with an elastic drip shield was used as an analogue for the increased rubble loads on the drip shield during vibratory ground motion. Table 2 presents the average pressures on the legs and top of the drip shield as a function of the density multiplier.

Table 2. Average Pressure Values on the Drip Shield as a Function of Rubble Density

Density Multiplier	Pressure (kPa)		
	Left Leg	Top (Crown)	Right Leg
1	41.99	127.86	61.87
2.5	69.86	263.73	80.98
3	82.98	314.81	89.54
4	105.74	415.97	109.03

Sources: SNL 2007a, Table 6-136, for a density multiplier of 1;
BSC 2004, Table 3, for density multipliers greater than 1.

Figure 1 is a plot of the data in Table 2. Figure 1 demonstrates that the variability of the vertical rockfall load is much greater than the variability of the lateral rockfall load as a function of the density multiplier. The assessment of the plastic load capacity of the drip shield framework (SNL 2007a, Sections 6.4.3.2.2.2 and 6.4.3.2.2.3) focuses on vertical loading because the vertical load on the crown is the driving force for lateral buckling of the sidewalls (as noted above) and because the average vertical rockfall load is significantly greater than the average lateral load, based on the results in Figure 1. Load realization 3 is then a reasonable choice for the maximum vertical rockfall load among the six realizations.

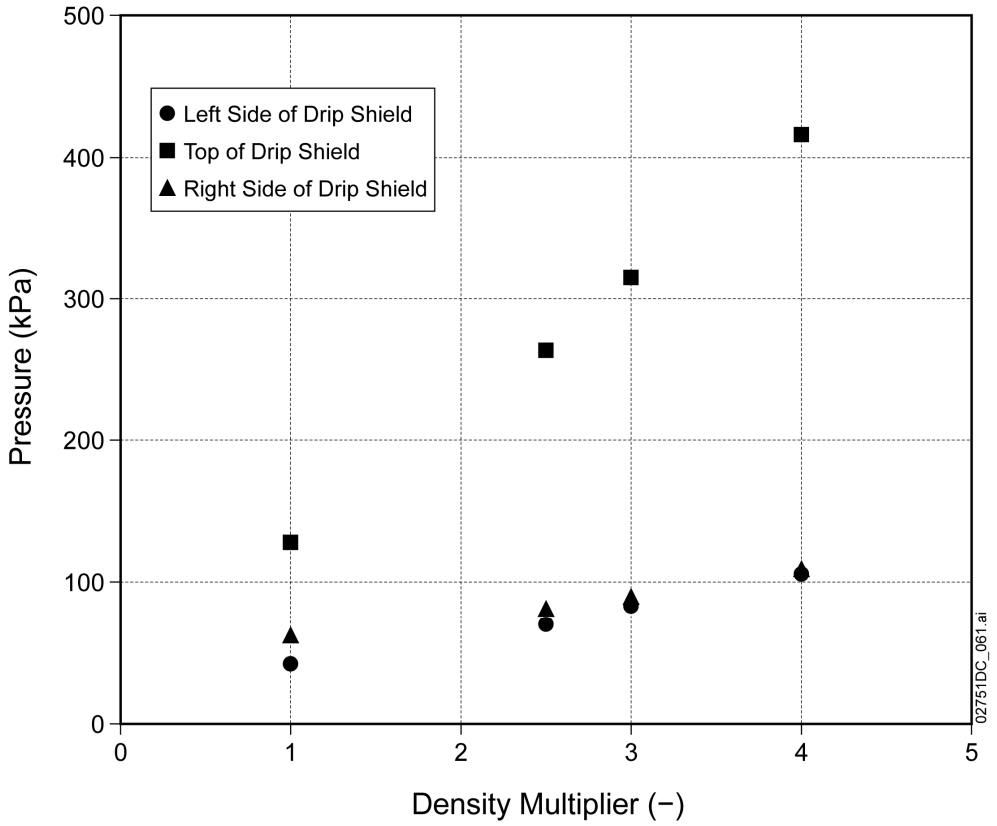

Figure 1. Average Rockfall Pressure on the Sides and Top of the Drip Shield as a Function of the Density Multiplier

1.2 UNCERTAINTY IS PROPAGATED INTO THE PLASTIC LOAD CAPACITY

The ultimate plastic capacity of the drip shield framework has been evaluated for thickness reductions of 0 mm, 5 mm, and 10 mm in all its structural components. These thickness reductions correspond to plate thicknesses of 15 mm, 10 mm, and 5 mm, respectively (SNL 2007a, Section 6.4.3). The resulting load capacities for the three drip shield configurations and the two load realizations are defined in Table 6-38 of *Seismic Consequence Abstraction* (SNL 2007b).

The uncertainty in the ultimate load capacity is represented as a log-normal probability distribution whose mean is defined by a least-squares fit to the load capacity for the mean load pattern. This is appropriate because the mean load pattern provides a reasonable estimate of the effective average load on the drip shield. The standard deviation of the probability distribution is defined by the maximum capacity difference for the two load patterns. Load realization 3, which has the highest vertical load on the crown of the drip shield for the six load realizations, provides a reasonable estimate for +1 standard deviation in the vertical load and is used to define +1 standard deviation for the plastic load capacity. Based on the data in Table 1, the mean vertical load on the crown plus one standard deviation is calculated to be (127.86 kPa + 19.40 kPa) = 147.26 kPa. This numerical value is about 5% less than the average vertical load on the crown for realization 3, which is 154.81 kPa. The structural response to load realization 3 therefore provides a slight overestimate for +1 standard deviation in the vertical load (calculated in Table 1).

Based on the computational results for the average load and for load realization 3, the values for the mean and standard deviation of the log-normal probability distribution, denoted as λ_{CAP} and β_{CAP}, respectively, have been evaluated at the three plate thicknesses (see Table 3). The largest value for β_{CAP}, 0.208, occurs for the 10 mm thickness reduction and has been used to represent uncertainty about the mean for all plate thicknesses. This approach significantly overestimates the uncertainty at smaller thickness reductions. For example, the value of $(\beta_{CAP})^2$ at 0-thickness reduction is 0.0020, with a corresponding value for β_{CAP} of 0.045, or about a factor of 4 less than the uncertainty that is incorporated into the log-normal distribution for plastic load capacity. This approach overestimates the probability of failure for a given static rockfall at a given vertical acceleration, as is evident in Figure 2, particularly because the variability of the log-normal distribution is much greater than the variability between data points for plate thicknesses of 10 mm and 15 mm, corresponding to thickness reductions of 5 mm and 0 mm, respectively.

Table 3. Log-Normal Parameters for the Ultimate Load Capacity of the Drip Shield Framework

Thickness Reduction (mm)	Thickness (mm)	Plastic Load Capacity for Mean Load Pattern (Pa)	Plastic Load Capacity for Realization 3 Pattern (Pa)	$(\beta_{CAP})^2$ (-)	Maximum Value of β_{CAP} (-)	λ_{CAP} (-)
10	5	500,800	606,200	0.0433	0.208	13.10
5	10	1,094,000	1,183,000	0.0066	0.208	13.88
0	15	1,698,000	1,622,000	0.0020	0.208	14.32

Source: SNL 2007b, Table 6-39.

NOTE: The mean value and standard deviation of the log-normal distribution are denoted as λ_{CAP} and β_{CAP}, respectively. The formulas for calculating λ_{CAP} and β_{CAP} are defined in the notes to Table 6-39 of SNL 2007b.

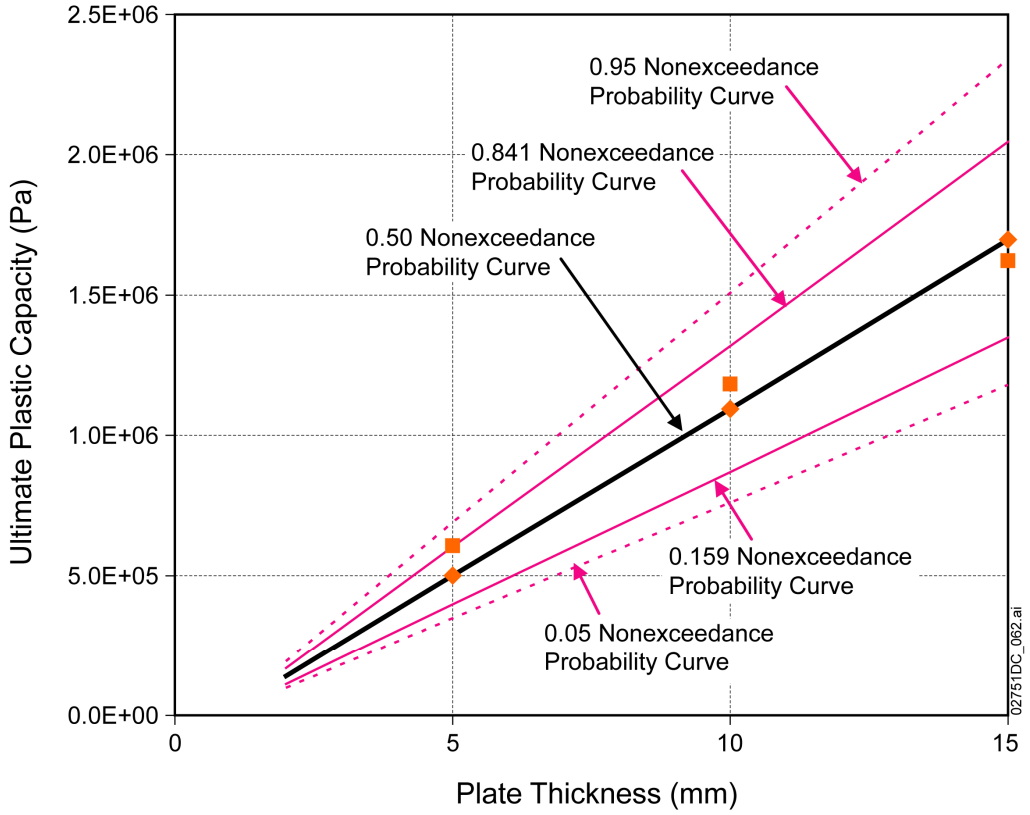

Source: SNL 2007b, Figure 6-73.

NOTE: Squares for realization 3 load pattern, diamonds for mean load pattern. The 0.841 and 0.159 percentiles represent ±1 standard deviation.

Figure 2. Comparison of Percentiles on the Log-Normal Distributions with the Calculated Plastic Load Capacity of the Drip Shield Framework

1.3 CONSISTENCY WITH RELATED FEPS

The analysis of loading uncertainty for the drip shield framework is not relevant to the screening justifications for excluded FEPs 2.1.07.05.0B, Creep of Metallic Materials in the Drip Shield; 2.1.03.03.0B, Localized Corrosion of Drip Shields; 2.1.06.05.0B, Mechanical Degradation of Invert; and 2.1.07.06.0A, Floor Buckling.

1.4 CONCLUSIONS

The effect of loading configuration uncertainty on the drip shield capacity is appropriately represented by the two load cases used in SAR Section 2.3.4.5.3.3.2. The average of the six quasi-static rockfall loads provides a reasonable representation of the average load on the drip shield framework and the structural response to this average load defines the mean of the probability distribution for plastic load capacity. Load realization 3 has the maximum vertical load and is used to define +1 standard deviation in the load pattern. This is a reasonable choice because the vertical load on the top (crown) is the driving force for lateral buckling of the sidewalls, because the average vertical rockfall load is significantly greater than the average lateral rockfall load, using dense rubble as an analogue for increasing dynamic loads, and because the magnitude of the vertical load on the crown for realization 3 is about 5% greater than +1 standard deviation above the mean for the six cases of vertical loading on the crown. The uncertainty in the plastic load capacity is propagated forward into the fragility curves in a manner that maximizes the variability for the 5 mm and 0 mm thickness reductions, as demonstrated by Figure 2.

2. COMMITMENTS TO NRC

None.

3. DESCRIPTION OF PROPOSED LA CHANGE

None.

4. REFERENCES

BSC (Bechtel SAIC Company) 2004. *Structural Stability of Drip Shield Under Quasi-Static Pressure*. 000-00C-SSE0-00500-000-00A. Las Vegas, Nevada: Bechtel SAIC Company. ACC: ENG.20040830.0032.

SNL (Sandia National Laboratories) 2007a. *Mechanical Assessment of Degraded Waste Packages and Drip Shields Subject to Vibratory Ground Motion*. MDL-WIS-AC-000001 REV 00. Las Vegas, Nevada: Sandia National Laboratories. ACC: DOC.20070917.0006.

SNL 2007b. *Seismic Consequence Abstraction.* MDL-WIS-PA-000003 REV 03. Las Vegas, Nevada: Sandia National Laboratories. ACC: DOC.20070928.0011.

RAI Volume 3, Chapter 2.2.1.3.2, Number 4:

Provide a technical basis to select the most severe loading configuration with respect to drip shield capacity based solely on the vertical loading, a selection that does not account for the potentially significant effects of lateral loads.

Basis: The applicant indicates that loading case 3 is the most severe among the six computed realizations (SAR Section 2.3.4.5.3.3.2) because case 3 has the highest average vertical load (SAR Section 2.3.4.5.3.2.1). Case 3, however, has one of the smallest lateral-to-vertical load ratios of the six cases (SNL 2007, Table 6.136). As observed in SAR Figure 2.3.4-83, this load configuration is not the most severe case for buckling failure (i.e., cases with plate thinning of 5 and 10 mm).

1. RESPONSE

While load realization 3 exhibits the maximum vertical rockfall load among the six load realizations, it is not envisioned to represent an extreme load for determining plastic load capacity. Load realization 3 is used to define +1 standard deviation in the load pattern and in the resulting plastic load capacity of the drip shield framework. The resulting distribution significantly overestimates the uncertainty for the plastic load capacity of the drip shield with 15-mm and 10-mm thick plates (no thickness reduction and 5-mm thickness reduction, respectively) because the variability for the 5-mm thick plate is much greater than the variability between data points for plate thicknesses of 10 mm and 15 mm, as explained in the response to RAI 3.2.2.1.3.2-003.

The results from quasi-static analyses have been used to develop a bounding representation of plastic load capacity for the framework fragility curves. The observation that load realization 3 has greater plastic load capacity than the mean load pattern for the corroded states of the drip shield indicates that lateral load has an influence on the bowing and buckling of the drip shield side walls in the quasi-static approach. On the other hand, fully coupled dynamic calculations with ground motions at the 2.44 m/s and 4.07 peak ground velocity (PGV) levels (SAR Section 2.3.4.5.3.3.3 and SNL 2007a, Section 6.4.4) demonstrate that the quasi-static approach provides a bounding approximation for plastic load capacity relative to fully coupled dynamic calculations. Given this result, the use of load realization 3 is appropriate for defining +1 standard deviation in the plastic load capacity.

1.1 RATIONALE FOR USING LOAD REALIZATION 3

The ultimate plastic load capacity of the drip shield framework (i.e., the limit load at which the framework fails) is based on two load distributions: (a) an average of the six quasi-static rockfall loads, and (b) the loads for realization 3, which was selected because it has the greatest load on the top (crown) of the drip shield (SNL 2007a, Section 6.4.3.2.2.2). Table 1 presents the static rubble loads on the left leg, top (crown), and right leg of the drip shield, the average values for the six static rockfall realizations, and the standard deviations for the six realizations.

Table 1. Average Pressure Values on the Drip Shield for Quasi-static Drift Degradation

Realization	Pressure (kPa)		
	Left Leg	Top (Crown)	Right Leg
1	41.54	108.91	58.76
2	19.15	147.07	19.33
3	31.35	154.81	6.69
4	57.23	129.75	128.81
5	69.69	112.73	105.43
6	32.97	113.87	52.19
Average	41.99	127.86	61.87
Standard Deviation	18.53	19.40	47.62

Source: Adapted from SNL 2007a, Table 6-136.

The choice of the average of the six quasi-static rockfall loads to represent the average load on the drip shield framework is straightforward and is not discussed further.

The choice of load realization 3 is motivated by two factors:

- The vertical load on the top (crown) is the driving force for lateral buckling of the sidewalls. The classical analysis for the buckling of a thin beam determines the stability of the beam under thrust (i.e., for a force parallel to the beam and applied at its end(s)). The corresponding load for buckling the sidewalls is the vertical load on the crown.

- The vertical rockfall load is significantly greater than the lateral rockfall load, using dense rubble as an analogue for increasing dynamic loads, as explained below.

Previous quasi-static calculations assessed the factor of safety of the drip shield under quasi-static pressure (BSC 2004, Section 6). For these quasi-static analyses, an increase in the density of rubble in the two-dimensional UDEC analysis of rubble loads on an elastic drip shield was used as an analogue for the increased rubble loads on the drip shield during vibratory ground motion. Table 2 presents the average pressures on the legs and top of the drip shield as a function of the density multiplier.

Table 2. Average Pressure Values on the Drip Shield as a Function of Rubble Density

Density Multiplier	Pressure (kPa)		
	Left Leg	Top (Crown)	Right Leg
1	41.99	127.86	61.87
2.5	69.86	263.73	80.98
3	82.98	314.81	89.54
4	105.74	415.97	109.03

Sources: SNL 2007a, Table 6-136, for a density multiplier of 1;
BSC 2004, Table 3, for density multipliers greater than 1.

Figure 1 is a plot of the data in Table 2. Figure 1 demonstrates that the variability of the vertical rockfall load is much greater than the variability of the lateral rockfall load as a function of the density multiplier. The assessment of the plastic load capacity of the drip shield framework (SNL 2007a, Sections 6.4.3.2.2.2 and 6.4.3.2.2.3) focuses on vertical loading because the vertical load on the crown is the driving force for lateral buckling of the sidewalls (as noted above) and because the vertical rockfall load is significantly greater than the lateral load, based on the results in Figure 1.

Load realization 3, which has the highest total load on the crown of the drip shield, is then a reasonable choice for the maximum rockfall load among the six realizations. Based on the data in Table 1, the mean vertical load on the crown plus one standard deviation is calculated to be (127.86 kPa + 19.40 kPa) = 147.26 kPa. This numerical value is about 5% less than the average vertical load on the crown for load realization 3, which is 154.81 kPa. The structural response to load realization 3 therefore provides a slightly conservative estimate for +1 standard deviation in the load capacity.

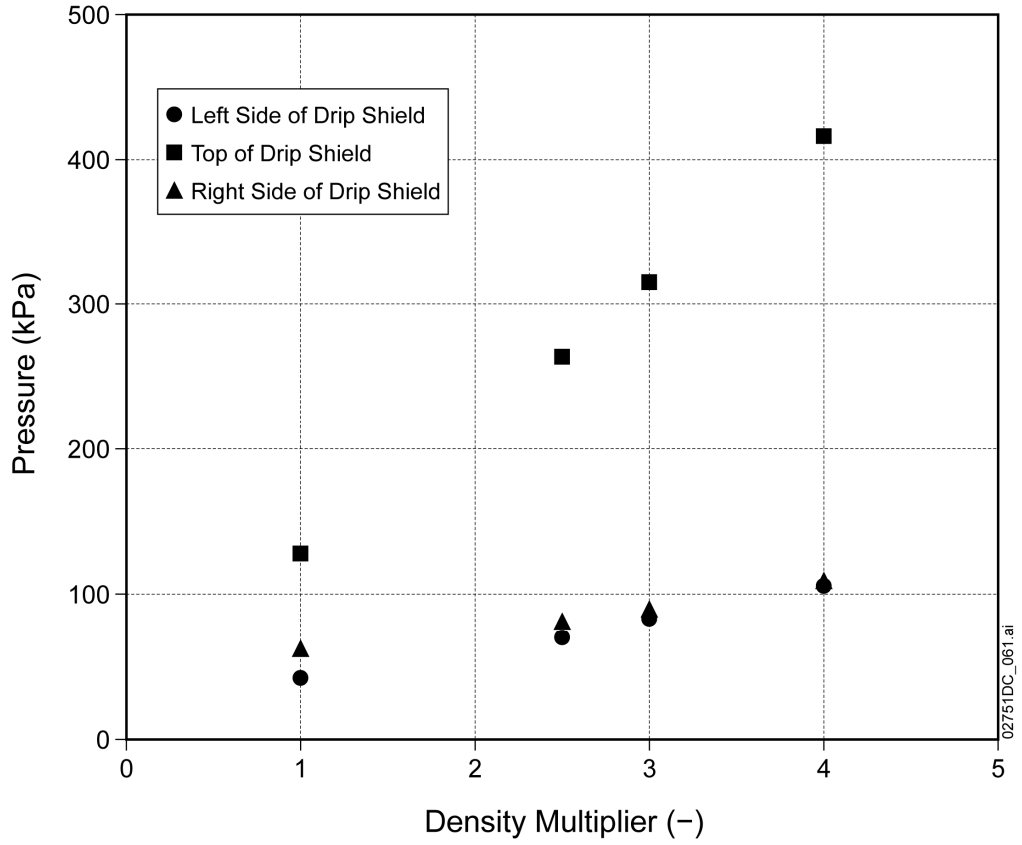

Figure 1. Average Rockfall Pressure on the Sides and Top of the Drip Shield as a Function of the Density Multiplier

While load realization 3 exhibits the maximum vertical rockfall load among the six load realizations, it is not envisioned to represent an extreme load for determining plastic load capacity. As noted in the basis to the RAI, SAR Figure 2.3.4-83 demonstrates that, compared to the mean load pattern, load realization 3 does not produce the lowest plastic load capacity for the drip shield framework with the 5-mm or 10-mm plate thicknesses. The source figure for SAR Figure 2.3.4-83 is reproduced in this response as Figure 2. Judging by the reversal in capacity between plate thicknesses of 10 mm and 15 mm for the two load patterns, the structural response of the drip shield framework changes between these plate thicknesses. This has been confirmed by the quasi-static calculations for plastic load capacity of the framework (SNL 2007b, Section 6.8.3.1), which are the basis for Figure 2. For the uncorroded drip shield with 15-mm plate thickness, the observed failure mode is snap-through of the crown of the drip shield. For the corroded states of the drip shield, the observed failure mode is buckling of the sidewalls of the drip shield. The snap-through failure mode should be directly influenced by vertical rockfall load, which has its greatest value for load realization 3. It is therefore reasonable that the plastic load capacity for load realization 3 is less than the plastic load capacity for the average of the six load realizations with an uncorroded drip shield. The observation that load realization 3 has greater plastic load capacity for the corroded states of the drip shield indicates that lateral load has an influence on the bowing and buckling of the drip shield side walls in the quasi-static analysis.

A series of fully coupled dynamic calculations with ground motions at the 2.44 m/s and 4.07 m/s peak ground velocity (PGV) levels were performed to further investigate the failure modes and failure loads obtained from the quasi-static analyses for plastic load capacity (SAR Section 2.3.4.5.3.3.3 and SNL 2007a, Section 6.4.4). These dynamic calculations demonstrated that buckling of the drip shield sidewalls is the main potential failure mode of the framework at all thicknesses because snap-through of the crown was not observed to occur. The dynamic calculations also demonstrated that the quasi-static approach is in agreement with the fully coupled dynamic approach or underestimates stability of the drip shield for strong ground motions (SNL 2007b, Section 6.4.4.6). In effect, the quasi-static approach provides a bounding approximation for plastic load capacity of the coupled rockfall-drip shield system during a seismic event.

In this situation, the quasi-static results provide a bounding representation of plastic load capacity for development of the framework fragility curves. As explained in the response to RAI 3.2.2.1.3.2-003, the log-normal distribution for plastic load capacity is based on the response for the mean load pattern and on the maximum standard deviation defined by load realization 3, which occurs for the 5-mm thick plate (10-mm thickness reduction). The resulting distribution for plastic load capacity significantly overestimates the uncertainty for the drip shield with 15-mm and 10-mm thick plates (no thickness reduction and 5-mm thickness reduction, respectively) because the variability for the 5-mm thick plate is much greater than the variability between data points for plate thicknesses of 10 mm and 15 mm (Figure 2 in the response to RAI 3.2.2.1.3.2-003 or SNL 2007b, Figure 6-73).

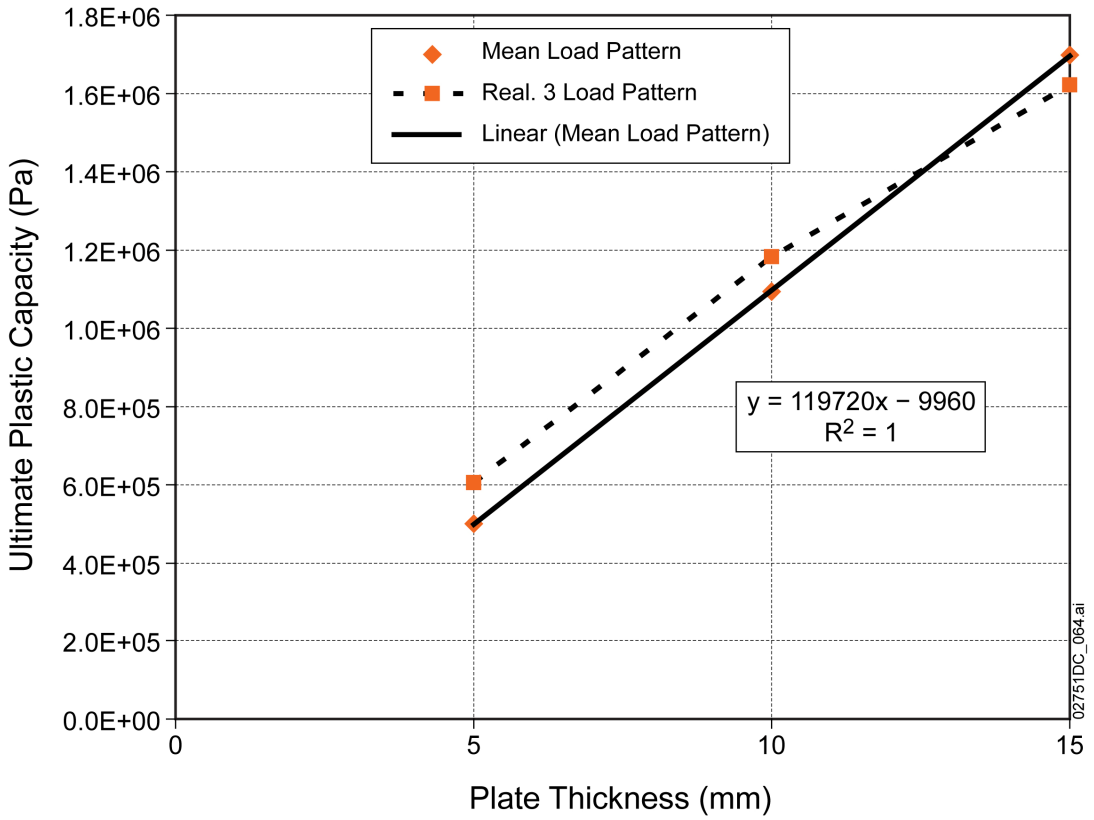

Source: SNL 2007b, Figure 6-72.

Figure 2. Plastic Load Capacity of the Drip Shield Framework as a Function of Plate Thickness and Boundary Conditions

1.2 CONSISTENCY WITH RELATED FEPS

The use of realization 3 to define the +1 standard deviation in the plastic load capacity is not relevant to the screening justifications for excluded FEPs 2.1.07.05.0B, Creep of Metallic Materials in the Drip Shield; 2.1.03.03.0B, Localized Corrosion of Drip Shields; 2.1.06.05.0B, Mechanical Degradation of Invert; and 2.1.07.06.0A, Floor Buckling.

1.3 CONCLUSIONS

The quasi-static calculations for plastic load capacity of the framework, which are the basis for Figure 2, have a change in failure mode between plate thicknesses of 10 mm and 15 mm. The observed failure modes are snap-through of the crown of the drip shield for the 15-mm thick plates and buckling of the sidewalls of the drip shield for the 5-mm and 10-mm thick plates. This change in quasi-static failure mode explains the crossing of the curves observed in Figure 2. The observation that load realization 3 has greater plastic load capacity for the corroded states of the drip shield indicates that lateral load has an influence on the bowing and buckling of the drip shield side walls in the quasi-static analysis.

A series of fully coupled dynamic calculations with ground motions at the 2.44 m/s and 4.07 peak ground velocity (PGV) levels were performed to further investigate the failure modes and failure loads obtained from the quasi-static analyses for plastic load capacity (SAR Section 2.3.4.5.3.3.3 and SNL 2007a, Section 6.4.4). These dynamic calculations demonstrated that buckling of the drip shield sidewalls is the main potential failure mode of the framework at all thicknesses because snap-through of the crown was not observed to occur. The dynamic calculations also demonstrated that the quasi-static approach provides a bounding approximation for plastic load capacity of the coupled rockfall–drip shield system during a seismic event.

In this situation, the quasi-static results have been used to develop a bounding representation of plastic load capacity. While load realization 3 exhibits the maximum vertical rockfall load among the six load realizations, it is not envisioned to represent an extreme load for determining plastic load capacity. Load realization 3 is used to define +1 standard deviation in the load pattern and the resulting plastic load capacity of the drip shield framework. This is a reasonable approach given the bounding nature of the quasi-static results. The resulting distribution for plastic load capacity significantly overestimates the uncertainty for the drip shield with 15-mm and 10-mm thick plates (no thickness reduction and 5-mm thickness reduction, respectively) because the variability for the 5-mm thick plate is much greater than the variability between data points for plate thicknesses of 10 mm and 15 mm, as explained in the response to RAI 3.2.2.1.3.2-003..

2. COMMITMENTS TO NRC

None.

3. DESCRIPTION OF PROPOSED LA CHANGE

None.

4. REFERENCES

BSC (Bechtel SAIC Company) 2004. *Structural Stability of Drip Shield Under Quasi-Static Pressure*. 000-00C-SSE0-00500-000-00A. Las Vegas, Nevada: Bechtel SAIC Company. ACC: ENG.20040830.0032.

SNL (Sandia National Laboratories) 2007a. *Mechanical Assessment of Degraded Waste Packages and Drip Shields Subject to Vibratory Ground Motion*. MDL-WIS-AC-000001 REV 00. Las Vegas, Nevada: Sandia National Laboratories. ACC: DOC.20070917.0006.

SNL 2007b. *Seismic Consequence Abstraction.* MDL-WIS-PA-000003 REV 03. Las Vegas, Nevada: Sandia National Laboratories. ACC: DOC.20070928.0011.

RAI Volume 3, Chapter 2.2.1.3.2, Number 5:

Demonstrate that additional deformation of drip shield due to the uneven degradation of the invert does not decrease the drip shield capacity. Also, provide the bearing capacity and settlement calculations for the invert.

Basis: SAR Section 2.3.4.5.3.1 indicates that uneven invert degradation would not decrease the drip shield vertical load carrying capacity. To support this conclusion, the applicant developed a model in which the drip shield is rotated as rigid-body prior to applying the static loading (SNL, 2007; Section 6.4.6.1). The drip shield rotation as a rigid body, however, does not account for the effect of additional deformation of drip shield components caused by uneven invert degradation.

1. RESPONSE

1.1 INTRODUCTION

Additional deformation of the drip shield due to the uneven degradation of the invert does not significantly decrease the drip shield capacity. It is demonstrated in this response that uneven degradation of the invert does not affect the drip shield fragility loaded by amplified rubble load due to seismic ground acceleration. It is also shown that a large safety factor of the drip shield for static rubble load compensates potential uneven load distribution and its uncertainties. The bearing capacity and settlement calculations of the invert are provided.

Analyses of drip shield stability when statically loaded by rubble due to drift collapse in the lithophysal rock mass (BSC 2004) and the drip shield framework fragility (SNL 2007a) were carried out assuming the drift invert on which the drip shield rests to be a flat, even, and rigid surface. The invert will be filled with compacted, initially leveled crushed tuff (Figure 1). A carbon steel substructure to be used during waste emplacement operations is embedded in the crushed tuff as shown in Figure 1, and is expected to corrode gradually.

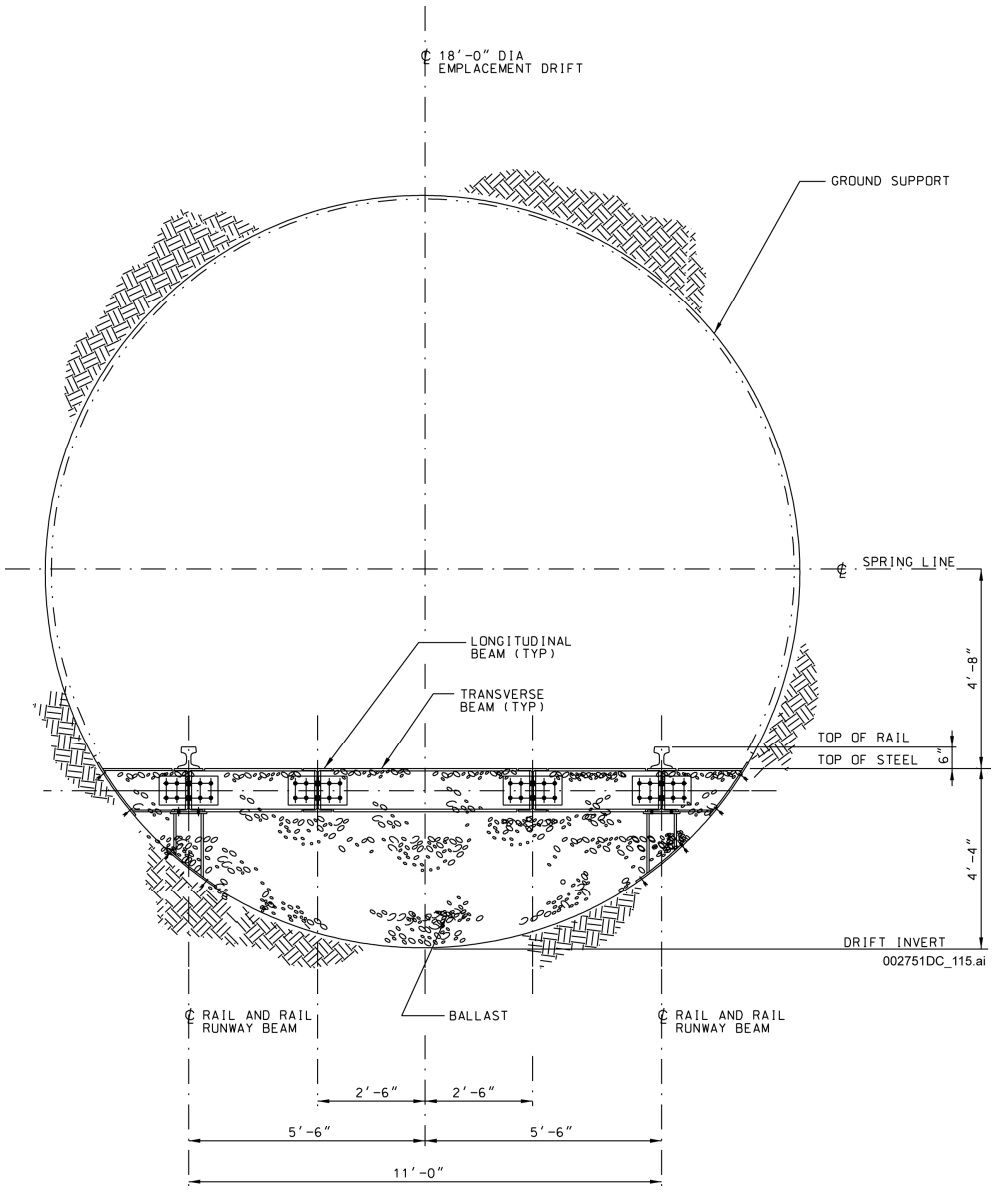

Figure 1. Drip Shield Support Elements in an Invert

Corrosion of the substructure and any settlement of the invert will probably not be spatially uniform. The bounding case, in which uneven settlement takes place in such a way that one side of the invert drops relative to the other uniformly over a sufficient distance that the entire drip shield tilts, is analyzed and the results are presented in *Mechanical Assessment of Degraded Waste Packages and Drip Shields Subject to Vibratory Ground Motion* (SNL 2007a, Section 6.4.6.1). It was shown that even for extreme assumptions of settlements up to 25 cm, the uneven settlement and tilting of the drip shield as a rigid body would not affect stability of the drip shield.

However, when uneven settlement takes place along a relatively short distance, smaller than the drip shield length, it can result in bridging of the drip shield over the sections where the invert settled more. In those situations, distribution of the potential rubble load between and along the drip shield legs (the sidewall and the support beams) and the bases will be uneven. If settlement is such that some of the support beams are not touching the invert, the load that should be carried by those support beams will be transferred to the adjacent support beams. Thus, as a result of uneven settlement and uneven load distribution, support beams carrying the larger loads can fail at smaller average pressures on the drip shield crown than in cases where the support beams are evenly loaded.

If the profile of invert is known, the effect of uneven settlement on structural response of the drip shield could be analyzed in a three-dimensional model of the entire drip shield. However, such analysis was not conducted because of large uncertainty in possible invert profiles. Uneven invert settlement could occur due to uneven degradation of the steel substructure. Seismic ground shaking could either cause uneven settlement or bulking of the crushed tuff in the invert. There is a high degree of uncertainty in the deformation of the invert as a function of time and location, since it will depend on the rate of steel corrosion, the frequency and magnitude of seismic events, and the evolution of the rubble accumulated on the crushed tuff in the invert and on the drip shield. Thus, the load distribution on the legs and the base will be variable. This effect is assessed by redistributing the load from the unloaded supports (resulting from the assumed uneven settlement) to the remaining support beams and the base resting on the invert.

The extent to which the uneven settlement can have an effect on uneven forces in the support beams can be affected by bearing capacity of the invert and potential penetration of the drip shield legs into the crushed tuff. Uneven forces on the drip shield legs and increased pressure in the base resting on the invert can cause penetration of the drip shield in the tuff, resulting in reduction of arching and more even load distribution.

1.2 DISCUSSION

1.2.1 Invert Bearing Capacity and Settlement Calculations

The analysis of the invert bearing capacity and settlement, when the steel substructure has corroded away, was carried out using numerical code FLAC Version 4.04 (STN: 10167-4.04-00). The problem was simulated as a rigid punch 75 mm wide, which is the width of the drip shield base. The punch indented into a half space—i.e., the crushed tuff in the invert, at a constant but small velocity (to ensure quasi-static conditions). The analyzed geometry and the displacement vector field at the end of simulation for one analyzed case (i.e., 50° friction angle of crushed tuff and with no surcharge pressure outside of the drip shield) are shown in Figure 2. The input parameters used in the calculations are listed in Table 1. The dilation angle was assumed in all calculations to be 10°, in general agreement with data in published literature (e.g., Korkiala-Tanttu and Laaksonen 2004, Table 2).

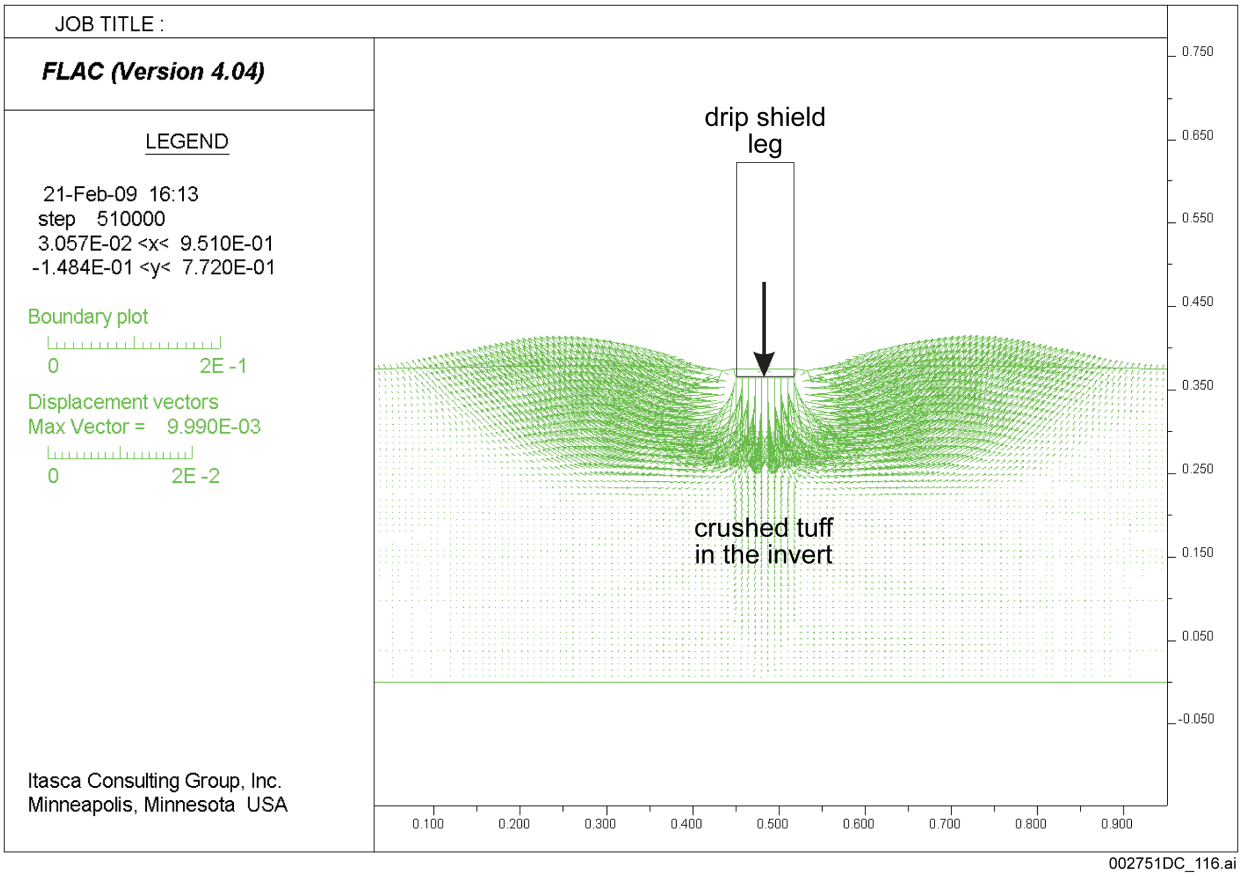

NOTE: The model does not extend to the rock boundary at the bottom. As long as the failure mechanism is contained within the model, as illustrated in the figure, the model size does not affect the bearing capacity solution.

Figure 2. Displacement Vector Field (m) at the End of Simulation for 50° Friction Angle and No Surcharge by the Rubble outside the Drip Shield

Table 1. Input Parameters Used in the Bearing Capacity and Settlement Calculations

Property	Value
Density	125 pcf ~ 2,000 kg/m^3
Friction angle	45°, 50°, and 55°
Shear modulus (G)	838,525 psf ~ 40 MPa
Poisson's ratio (ν)	0.23
Bulk modulus (K) $K = \frac{2G(1+\nu)}{3(1-2\nu)}$	60.7 MPa

The analyses were carried out for three values of friction angle listed in Table 1. (Friction angles less than 45° are typical of minimum test results at large confining stresses of the order of 1 MPa. Thus, friction angles less than 45° were not considered in the analysis. Because bearing capacity is insensitive to values of shear modulus and Poisson's ratio, only one set of values was used in the analysis.) Two cases were considered: (1) open drift and no surcharge on the invert surface on both sides of the leg (i.e., the drip shield leg on the free surface of the invert), and (2) collapsed drift with a surcharge pressure of accumulated rubble between the drip shield leg and the drift wall. The surcharge pressure, applied on the outside of the drip shield leg, is taken to be 127.86 kPa, which is the mean pressure on the drip shield crown calculated from the six rubble load realizations (SNL 2007a , Table 6-136). Any effect of surcharge pressure of the waste package and the pallet inside the drip shield is neglected in the calculations, which will result in underestimating bearing capacity.

Calculated pressures at the bottom of the drip shield base as functions of the vertical displacement are obtained from the calculations. The results for three different friction angles and two conditions of rubble pressure are summarized in Figure 3. The results for the case without surcharge pressure are in good agreement with the soil mechanics formula for bearing capacity of shallow foundations. For example, the formula for bearing capacity, q_{ult} (Bowles 1996, Hansen's equation, Table 4-1, simplified for cohesionless soil, assuming infinitely long foundation on flat soil surface loaded by vertical force only):

$$q_{ult} = \frac{1}{2}\gamma B N_{\gamma} \qquad \text{(Eq. 1)}$$

where γ is the unit weight, B is the width of footing, and N_{γ} is the bearing capacity factor, yields for friction angle of 45° (and $N_{\gamma} = 200.5$, Bowles 1996), $q_{ult} = 150$ kPa. The maximum pressure calculated from numerical simulation for the same case is 162 kPa (Figure 3). The results indicate increase in bearing capacity with increase in the friction angle. Also, the surcharge pressure results in increase in the bearing capacity of the crushed tuff.

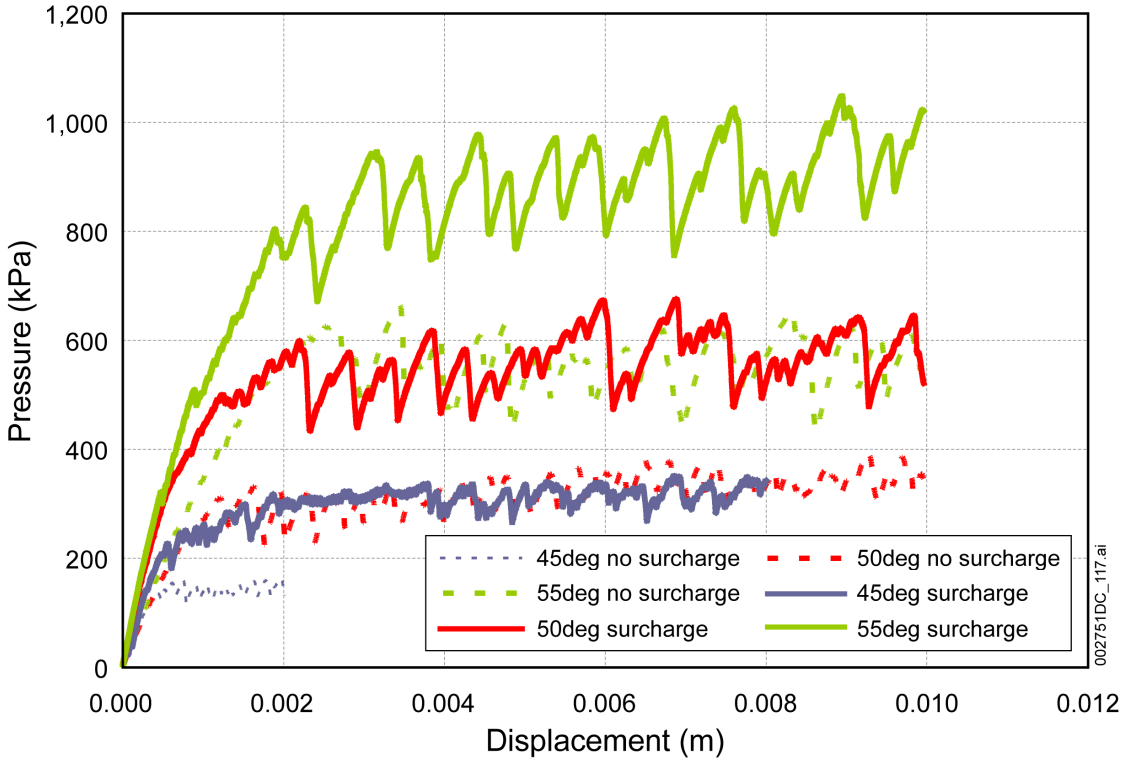

Figure 3. Results of Bearing Capacity Calculations (pressure versus displacement) for Different Friction Angles and Assumptions of Rubble Surcharge Pressure

The drip shield loads on the crushed tuff in the invert were also calculated for two states of the emplacement drift: (1) open drift, and (2) collapsed drift, when the rubble has accumulated along the legs and on the drip shield crown. For the collapsed drift, the average of the six realizations of rubble load on the drip shield (SNL 2007a, Table 6-136) was used in the analysis—the pressure on the crown of 127.86 kPa, and 41.99 kPa and 61.87 kPa on the left and right legs, respectively. The input parameters used in the calculations of the drip shield pressures on the crushed tuff in the invert are listed in Table 2.

Table 2. Input Parameters Used in Calculation of the Drip Shield Pressure on Invert

Input Parameter	Value
Drip Shield Weight	5,000 kg
Drip Shield Length	5.805 m
Drip Shield Shoulder Height	2.209 m
Drip Shield Shoulder Width	2.280 m

The pressure on the invert, q_{DS}, due to drip shield only—i.e., in the case of free standing drip shield—is calculated as follows:

$$q_{DS} = \frac{Mg}{BL} = \frac{5,000 \times 9.81}{2 \times 5.805 \times 0.075} = 56 \text{ kPa} \quad \text{(Eq. 2)}$$

where $M = 5,000$ kg is the drip shield mass; $g = 9.81 \text{m/s}^2$ is gravity acceleration; $B = 2 \times 0.075$ m is the width of the two bases below the drip shield legs; and $L = 5.805$ m is the drip shield length.

The pressure on the invert, q_R, due to accumulated rubble is estimated as follows:

$$q_R = \frac{p_c \frac{W_{DS}}{2} - \frac{p_{ll} + p_{lr}}{2} H_{DS} F_c}{B} = \frac{127.86 \frac{2.280}{2} - \frac{41.99 + 61.87}{2} 2.209 \times 0.8}{0.075} = 720 \text{ kPa} \quad \text{(Eq. 3)}$$

Where $p_c = 127.86$ kPa, $p_{ll} = 41.99$ kPa, and $p_{lr} = 61.87$ kPa are the rubble pressures on the crown and legs of the drip shield (SNL 2007a, Table 6-136); $W_{DS} = 2.280$ m is the width of the drip shield crown; and $H_{DS} = 2.209$ m is the height of the drip shield crown. F_c is the friction coefficient between titanium of the drip shield legs and the rubble accumulated along the legs, assumed in this calculation to be 0.8. The friction coefficient of the metal-to-rock surfaces are typically in the range between 0.2 and 0.8 (SNL 2007a, Section 5.4). The upper bound of the range is selected to take into account that the outside surface of the drip shield leg has lifting feature assemblies and external plates that will vertically support the drip shield on rubble pressing against the drip shield sides.

The pressure of the drip shield leg and the base on the crushed tuff in the invert when the drift is open and the drip shield is standing free on the invert is smaller than the bearing capacity of the crushed tuff even in the case of a friction angle of 45°. Thus, the invert will carry the drip shield, when the steel substructure has corroded away, with relatively little settlement.

When the drifts collapse, the estimated total pressure of the drip shield on the invert (assuming the average of the six rubble load realizations):

$$q = q_{DS} + q_R = 56 + 720 = 776 \text{ kPa} \quad \text{(Eq. 4)}$$

exceeds the bearing capacity of the invert (accounting for the surcharge pressure on one side) for the friction angles of 45° and 50°, but is less than the bearing capacity for a friction angle of 55° (~1,000 kPa in Figure 3). Considering the weight of the waste package and the pallet inside the drip shield (not taken into account as the surcharge pressure) and the weight of the rubble outside the drip shield, the invert tuff is anticipated to be well compacted when the rubble accumulates. For those conditions, a friction angle of 55° can be expected for the invert tuff. However, as explained in what follows, if the drip shield pressure on the invert exceeds the bearing capacity of the crushed tuff, the drip shield will penetrate some distance into the crushed tuff, but not all

the way to the solid rock in the invert of the emplacement drift. The drip shield penetration will be limited because this simple conservative model (based on comparison of the base pressure with the bearing capacity) does not represent increase in the resistance to penetration due to: (1) additional compaction of the crushed tuff under the drip shield legs, (2) more uniform distribution of the pressure and, consequently, reduction in the pressure on the tuff (i.e., bridging over more settled area of the invert will be reduced or eliminated), and (3) rubble support of the drip shield on the external support plates and lifting assemblies. Subsidence and penetration of the drip shield into the invert will also reduce the vertical load of rubble on the drip shield crown. Although the rubble load on the drip shield crown was conservatively assumed to be a dead load, it is not. Deformation of the drip shield will cause stress redistribution in the rubble and will increase stress arching above the drip shield and reduce rubble load on the drip shield.

1.2.2 Effect of Uneven Degradation of Invert on the Drip Shield Capacity

The purpose of the drip shield framework fragility calculations (SNL 2007a, Section 6.4.3.2) is to determine a vertical failure load for use in *Seismic Consequence Abstraction* (SNL 2007b). This failure load can be correlated to the ground motion peak ground acceleration (PGA) in order to determine a probability distribution for the ground motion intensity or the peak ground velocity (PGV) level at which the framework collapses. In the quasi-static analysis, the vertical load on the drip shield crown was gradually increased until the drip shield, assumed to be resting on the rigid leveled invert, failed. During strong seismic ground motions (e.g., the 2.44 m/s PGV level with a mean annual probability of recurrence of 4.5×10^{-7}), the drifts collapse and the drip shield and surrounding rubble undergo transient motions and interaction. The crushed tuff in the invert can be deformed, and the drip shield can be lifted off the invert by inertial forces. Thus, the initial uneven degradation and settlement of the invert will likely be inconsequential for the drip shield response during strong seismic ground shaking. Because a large volume of rubble will form above the drip shield, the main mechanism of drip shield failure is assumed to be amplification of the vertical load due to accumulated rubble above the drip shield by the vertical acceleration of a ground motion. The quasi-static model used in the drip shield framework analysis approximates that main mechanism. Conservatism of the quasi-static approach is demonstrated by comparison with the results of the dynamic simulations of drip shield–rubble interaction for the most intense ground motions at the 2.44 m/s and 4.07 m/s PGV levels (SNL 2007a, Section 6.4.4). Thus, uneven invert degradation has no effect on the results of drip shield fragility calculations.

The drip shield deformation and stability under static rubble load (BSC 2004) was conducted assuming the drip shield resting on the rigid, leveled invert. The calculations were carried out for a single drip shield segment assuming that loading and boundary conditions are uniform along the entire drip shield length. However, non-uniform invert degradation along the drip shield can cause non-uniform distribution of the load between the drip shield frameworks and support beams. Under such conditions, the more loaded portion of the drip shield framework and support beams will fail at smaller average vertical loads than for the uniform conditions. Because of uncertainties in non-uniform steel corrosion rates, loading conditions (i.e., intensity and duration of seismic ground motions), and rate of rubble accumulation, it is difficult to predict spatial and temporal evolution of the invert surface.

For this reason, factor-of-safety calculations for the drip shield load bearing capacity were carried out (BSC 2004). The density of the rubble accumulated above and along the sides of the drip shield was increased until the drip shield failed. The calculation shows that increasing the rubble density by a factor of 4 results in incipient failure (by buckling of the drip shield legs) of the drip shield (BSC 2004, Figure III-16). The calculation was carried out using the average of six load realizations. The average is more representative than any of the six realizations, because load distributions along the entire drip shield are considered. The average vertical load when the density is increased four times is 415.97 kPa (BSC 2004, Table 3). As the average vertical pressure on crown for nominal rubble density is 127.86 kPa (SNL 2007a, Table 6-136), the factor of safety is at least 3.3. The following is a simple estimate of the proportion of the surface, p, below the drip shield legs that can subside (degrade) before the loaded drip shield framework fails:

$$p = \frac{F_s - 1}{F_s} \qquad \text{(Eq. 5)}$$

where F_s is the factor of safety for a uniformly loaded drip shield. In the case of a factor of safety of 3.3, almost 70% of the invert can subside, leaving the drip shield to rest on remaining 30% before the loaded drip shield framework would fail (i.e., the legs buckle). Thus, the estimated factor of safety provides a large margin to cover uncertainties in the uneven invert degradation.

When the steel substructure in the invert completely corrodes away, the bearing capacity of the crushed tuff in the invert, which is relatively close to the drip shield pressure when drifts collapse (Section 1.2.1), will limit the proportion of the drip shield base that is not resting on the invert. When the drip shield pressure on the crushed tuff exceeds the crushed tuff bearing capacity, the drip shield will penetrate into the invert and reduce the proportion of the drip shield base, which is not resting on invert. The limiting proportion of the drip shield base not resting on the invert can be estimated as:

$$p = 1 - \frac{q}{q_{ult}} \qquad \text{(Eq. 6)}$$

In the case of $q = 776$ kPa and $q_{ult} = 1000$ kPa (Section 1.2.1), the proportion is estimated to be $p = 0.22$, resulting in a relatively small increase in the load due to uneven invert settlement.

1.3 CONSISTENCY WITH RELATED FEPS

The analysis of the drip shield load bearing capacity under static and dynamic loads, and for creep deformation of the drip shield, assumes that the drip shield is standing on flat, rigid invert. This is a physically reasonable approach for the drip shield capacity assessment. This approach is not relevant to the screening justifications for excluded FEPs 2.1.07.05.0B, Creep of Metallic Materials in the Drip Shield; 2.1.03.03.0B, Localized Corrosion of the Drip Shield; 2.1.06.05.0B, Mechanical Degradation of Invert; and 2.1.07.06.0A, Floor Buckling.

1.4 CONCLUSION

Accumulation of rubble sufficient to cover the drip shield, and particularly to load the drip shield at the level comparable to the pressures from the six rubble load realizations (SNL 2007a, Table 6-136), will occur as a consequence of low probability seismic events (greater than the 1 m/s PGV level; SNL 2007b, Figure 6-57), and a completely collapsed drift is an unlikely configuration in the first 10,000 years when only minimal rockfall will occur. Uneven invert degradation will not have an effect on the fragility of the drip shield loaded by rubble during strong seismic ground motions.

A large factor-of-safety of the drip shield to structural collapse when statically loaded by rubble load (i.e., the six static rubble load realizations, which also have low probability to develop in first 10,000 years) has been shown to account for significant uncertainty in uneven invert subsidence/degradation. When the steel substructure of the invert corrodes away, the bearing capacity of the crushed tuff in the invert will limit the extent of uneven load redistribution and the effect of uneven invert settlement, making these processes inconsequential to drip shield load bearing capacity.

2. COMMITMENTS TO NRC

None.

3. DESCRIPTION OF PROPOSED LA CHANGE

None.

4. REFERENCES

Bowles, J.E. 1996. *Foundation Analysis and Design*. 5th Edition. New York, New York: McGraw-Hill.

BSC (Bechtel SAIC Company) 2004. *Structural Stability of a Drip Shield Under Quasi-Static Pressure*. 000-00C-SSE0-00500-000-00A. Las Vegas, Nevada: Bechtel SAIC Company. ACC: ENG.20040830.0032; ENG.20080312.0017.

Korkiala-Tanttu, L. and Laaksonen, R. 2004. "Modelling of the Stress State and Deformations of APT Tests." In Proc. of the *2nd International Conference on Accelerated Pavement Testing*, September 26.9.–29.9.2004, Minneapolis, Minnesota. CD-ROM proceedings. B. Worel, ed. 22 pp.

SNL (Sandia National Laboratories) 2007a. *Mechanical Assessment of Degraded Waste Packages and Drip Shields Subject to Vibratory Ground Motion*. MDL-WIS-AC-000001 REV 00. Las Vegas, Nevada: Sandia National Laboratories. ACC: DOC.20070917.0006; DOC.20080623.0002; DOC.20081021.0001.

SNL 2007b. *Seismic Consequence Abstraction*. MDL-WIS-PA-000003 REV 03. Las Vegas, Nevada: Sandia National Laboratories. ACC: DOC.20070928.0011.